

# The Nuclear Stellar Cluster in the Seyfert 1 Galaxy NGC 3227: High Angular Resolution NIR Imaging and Spectroscopy

E. Schinnerer

*Astronomy Department, California Institute of Technology, Pasadena, CA 91125*

*MPI für extraterrestrische Physik, Giessenbachstrasse, 85748 Garching, Germany*

es@astro.caltech.edu

A. Eckart

*I. Physikalisches Institut, Universität zu Köln, Zùlpicherstraße 77, 50937 Köln, Germany*

*MPI für extraterrestrische Physik, Giessenbachstrasse, 85748 Garching, Germany*

eckart@zeus.ph1.uni-koeln.de

and

L.J. Tacconi

*MPI für extraterrestrische Physik, Giessenbachstrasse, 85748 Garching, Germany*

linda@mpe.mpg.de

## ABSTRACT

Near-Infrared high angular resolution speckle imaging and imaging spectroscopy of the nuclear region ( $\sim 10'' \approx 840$  pc) of the Seyfert 1 galaxy NGC 3227 are presented. The images reveal an unresolved nuclear source in the  $K$  band in addition to a nuclear stellar cluster which is slightly resolved in the  $J$  and  $H$  band. The contribution of this stellar cluster to the NIR continuum is increasing from the  $K$  to the  $J$  band. The stellar absorption lines are extended compared to the neighboring continuum suggesting a nuclear stellar cluster size of  $\sim 70$  pc FWHM. Analysis of the stellar absorption lines suggests that the stars are contributing about 65% (40%) of the total continuum emission in the  $H$  ( $K$ ) band in a  $3.6''$  aperture. The dominant stellar type are cool M type stars. Population synthesis in conjunction with NIR spectral synthesis indicates that the age of the mapped nuclear stellar cluster is in the range of 25 to 50 Myr when red supergiants contribute most to the NIR light. This is supported by published optical data on the Mg I  $b$  line and the CaII triplet. Although a higher age of  $\sim 0.5$  Gyr where AGB stars dominate the NIR light can not be excluded, the observed parameters are at the limit of those expected for a cluster dominated by AGB stars. However, in either

case the resolved stellar cluster contributes only about  $\sim 15\%$  of the total dynamical mass in the inner 300 pc. This immediately implies at least another much older stellar population which contributes to the mass but not the NIR luminosity. Pure constant star formation over the last 10 Gyr can be excluded based on the observational fact that in such a scenario the total observed (spatially unresolved and spectrally resolved) Br $\gamma$  flux would be of stellar origin which is spatially extended. Therefore, at least two star formation/starburst events took place in the nucleus of NGC 3227. Since such sequences in the nuclear star formation history are also observed in the nuclei of other galaxies a link between the activity of the star formation and the AGN itself seems likely.

*Subject headings:* galaxies: Seyfert – galaxies: nuclei – galaxies: ISM – galaxies: individual(NGC 3227)

## 1. INTRODUCTION

The nuclear stellar properties of Seyfert galaxies are of great interest, since there might be a connection between the nuclear star formation and the AGN activity (Norman & Scoville 1988). Current scenarios for fueling the nuclear region involve nuclear bars (e.g. Shlosman, Frank & Begelman 1989). However, recent high-angular resolution observations of Seyfert galaxies do not find enough evidence for this model (Regan & Mulchaey 1999, Malkan, Gorjian & Tam 1998). The nuclear star formation activity and the AGN both use the same fuel – the circumnuclear molecular gas. Detailed analysis of the nuclear stellar properties of the two Seyfert galaxies Circinus (Maiolino et al. 1998) and NGC 1068 (Thatte et al. 1997) have shown that the nuclear stellar clusters have age of  $\sim 10^8$  yr. This suggests that at least some of the molecular gas reaching the inner few 100 pc is converted into stars rather than being funneled directly to the AGN. In addition there might be an interplay between the star formation and the AGN classification (Ohsuga & Umemura 1999).

High angular resolution observations in the near-infrared (NIR) of the nuclear region of active galaxies are well-suited to investigate this problem via a quantitative analysis of the contributions of the AGN and the stars to the nuclear NIR continuum. The NIR offers two advantages over the optical wavelength ranges: (1) the extinction affecting the stellar light is much smaller (about 1/10 in the  $K$  band compared to the  $V$  band) and (2) the overall stellar contribution to the continuum emission is larger due to the spectral energy distribution (SED) of the AGN and the stars (e.g. Barvainis 1989). This allows for a more detailed analysis of the properties of the stellar contribution to the nuclear light. The combination of imaging spectroscopy with high angular resolution imaging is ideal to disentangle the contribution of the AGN from those of the stars using spectral and spatial information. The utilization of population synthesis and NIR spectral synthesis models allows to analyze the star formation history of the nuclear stellar component. NGC 3227, a nearby Seyfert 1 galaxy, was chosen for such a detailed study, since complementary data from other wavelengths are

already available in the literature.

NGC3227 (Arp 94b; type SAB pec, de Vaucouleurs et al. 1993) is a Seyfert 1 galaxy located at a distance of 17.3 Mpc (group distance; Garcia 1993;  $1'' \sim 84$  pc) and interacting with its elliptical companion NGC 3226. Rubin & Ford (1968) studied the system NGC 3226/7 for the first time in the optical. In NGC 3227 they found indications for a nuclear outflow as well as a spiral arm that stretches toward the close elliptical companion. The nucleus of NGC 3227 exhibits clear signs of Seyfert 1 activity. The Narrow Line Region (NLR) is extended towards the northeast (Mundell et al. 1992a, Schmitt & Kinney 1996). The Broad Line Region (BLR) clearly shows variations in the optical continuum and line emission (Salamanca et al. (1994). Mundell et al. (1995b) detected a double radio source with a separation of  $0.4''$  at a PA of  $\sim 10^\circ$ . The cold molecular gas traced by its  $^{12}\text{CO}$  line emission shows a circumnuclear ring with a diameter of  $\sim 3''$  plus weaker emission at the dynamical center. In the inner arcsecond strong non-circular motions are observed. Modeling of the kinematics indicates that a warped thin molecular gas disk can explain the observed kinematics quite well (Schinnerer, Eckart & Tacconi 1999, 2000). Optical and NIR observations (Mulchaey, Regan, Kundu 1997, De Robertis et al. 1998) indicate that the galaxy has a bar with  $R \approx 6.7 - 8.4$  kpc and a position angle of about  $-20^\circ$  relative to the major kinematic axis.

In this paper we present the first quantitative analysis of the AGN and stellar contributions to the nuclear NIR continuum of NGC 3227 using high angular NIR imaging and integral field spectroscopy. We describe our observations in §2, and discuss the results from the integral field spectroscopy in §3. The nuclear stellar content is derived in §4. We present an analysis of the high angular resolution imaging data in §5. Population synthesis and NIR spectral synthesis models are used in §6 to analyze the nuclear star formation history of NGC 3227. A description and discussion of these models is given in the appendix. A brief summary is presented in §7.

## 2. OBSERVATIONS

### 2.1. NIR imaging spectroscopic data

NGC 3227 was observed with the MPE integral field spectrograph 3D in the  $H$  and  $K$  band during two observing runs in January 1995 at the 3.5 m telescope on Calar Alto, Spain, and in December 1995/January 1996 at the William-Herschel-Telescope (WHT) at La Palma, Spain (Table 1). The spectral resolution was  $R = \frac{\lambda}{\Delta\lambda} \approx 750$  for the  $K$  band and  $\approx 1000$  for the  $H$  band. 3D (Weitzel et al. 1996) was used together with the tip-tilt corrector ROGUE (Thatte et al. 1995). 3D obtains simultaneous images and spectra over an  $8'' \times 8''$  field. This is done using an image slicer which rearranges the two-dimensional focal plane onto a long slit. A grism is used for dispersion and the spectra are then detected on a NICMOS 3 array. A detailed description of the instrument and the data reduction is given by Weitzel et al. (1996).

The data reduction procedure converts each two dimensional image into a three dimensional data

cube with two spatial axes and one spectral axis. The data cubes are co-added and centered on the continuum peak. All images are dark-current and sky-background subtracted, corrected for dead and hot pixels, and spatially and spectrally flat-fielded. To correct the effects of the Earth’s atmosphere to the  $H$  and  $K$  band spectrum, a standard star was observed. This standard spectrum was first divided by a template spectrum of the same spectral type (Kleinmann & Hall 1986) in order to remove stellar features. In the  $H$  band standard star observations could not be obtained for one night. We therefore used the model atmosphere from ATRAN for correction. Since the correction is only reliable for the central wavelength range ( $1.5196 \mu\text{m} - 1.7248 \mu\text{m}$ ), we discarded the remaining parts of the band. The effect due to different zenith distance of source and standard star was minimized using the ATRAN atmospheric model (Lord 1992), mainly to correct for the different atmospheric absorption. The source data were then divided by the resulting atmospheric transmission spectrum.

The flux calibration was done in a  $4.6''$  aperture using the flux measurement from our high resolution imaging SHARP data. From a comparison with the reference star and with the SHARP data we estimate that the achieved spatial resolution is  $\sim 1.6''$  FWHM and  $\sim 1.3''$  FWHM for the  $H$  and  $K$  band, respectively. The absolute flux calibration uncertainties are  $\sim 10\%$ . The uncertainties for the line fluxes given in Tables 3 and 4 include the noise in the line map as well as uncertainties due to the choice of the baseline and absolute flux calibration uncertainties. The total uncertainty amounts to about 13%. For the lines close to  $2.00 \mu\text{m}$  the uncertainties are larger due to the larger uncertainties induced by the low atmospheric transmission. Due to different implementations of the  $K$  band grism in the two observing runs the coverage of the  $K$  band differed slightly resulting in lower S/N at the beginning and the end of the spectral band.

## 2.2. NIR speckle data

NGC 3227 was observed in the  $J$ ,  $H$  and  $K$  band with the MPE speckle camera SHARP1 mounted to the ESO New Technology Telescope (NTT) at La Silla, Chile, on four nights in June 1996 (Table 1). SHARP1 has a  $12.8'' \times 12.8''$  field of view with a pixel scale of  $0.05''/\text{pixel}$ . The star 35 Leo served as a flux calibrator and a PSF reference. The images were sky-background subtracted, corrected for dead pixels and flat-fielded, and then co-added after re-centering with respect to each other using a simple shift and add (SSA) algorithm (Christou 1991). The nucleus of NGC 3227 was alternately positioned in one of the four quadrants of the NICMOS3 detector. The resulting images at different positions were mosaiced to obtain a larger FOV. The integration times per frame ranged from 0.5s ( $H$ ,  $K$  band) to 1.5s ( $J$  band) for NGC 3227 and from 0.25s ( $K$  band) to 0.5s ( $H$ ,  $J$  band) for 35 Leo. At each position about 300 frames were taken leading to an average integration time of  $\sim 3$  minutes (per SSA image) for both, NGC 3227 and 35 Leo.

*The stability of the PSF:* For a reliable estimate of the nuclear size of NGC 3227, good knowledge of the stability of the PSF is necessary. The PSF standard star is located about  $5^\circ$  away from NGC 3227 which is sufficiently close to monitor the same atmospheric conditions. The standard

star 35 Leo was observed at least ones per band, either at the beginning or end of the source observations each night. The total duration of the observation per band and night ranged from 20 to 75 minutes. To verify that the seeing was stable, we measured the FWHM in the individual SSA images of NGC 3227 and 35 Leo for each night. The FWHM within each band was found to be stable and the observed differences between NGC 3227 and 35 Leo were similar for all the nights. Therefore the seeing was stable during the observations and better than 1" in the visible (see Table 1):

Uncertainties in the PSF due to different frame integration times for NGC 3227 and 35 Leo can be excluded: The integration time per single frame ranged from 0.25s to 1.5s which is still short enough to obtain only a small number of speckles per frame, since the atmospheric coherence time in the  $K$  band lies between 30ms to 100ms (Hofmann et al. 1995). Different integration times (per frame) for NGC 3227 and the star (up to three times longer) might be considered as a cause for instability. However, comparison of our  $K$  band data with the same integration time used for NGC 3227 and the standard star, and different integration times used for both showed no difference in the obtained results. The seeing is expected to be better at longer wavelengths, since the atmospheric variations are slower and the monitoring is easier (see Table 1). All the above tests make us confident that the observations of 35 Leo gave a stable and reliable PSF for the NGC 3227 data.

The relative uncertainties in the flux calibration of the individual nights, and NIR bands amount to (5 - 8)%. Including systematic uncertainties (differences between color systems and filter curves) we estimate the total uncertainty for the flux calibration to be  $\sim 10\%$ . Comparison of the calibrated SSA mosaics (Table 5) and calibrated direct imaging data with a larger field of view (McAlary et al. 1983, Kotilainen et al. 1992) yields agreement to within  $0.15^{mag}$ .

The achieved angular resolution is 0.55" FWHM in the  $J$  band and 0.35" FWHM in the  $H$  and  $K$  band as measured from the reference star.

### 2.3. HST $V$ band image

The HST F606W image of NGC 3227 (P.I. Malkan) is saturated in the nucleus. We extracted the PC1 chip part with a pixel scale of 0.0455"/pixel. The image was corrected for dead pixel and remaining 'hot' pixel were removed by hand. The resolution in the HST image is 0.13" as obtained from a Gaussian fit to the northern knot (see section 5.1, Fig. 7). The correct center position was obtained by aligning the HST image with respect to the SHARP1 data. For this purpose the data were smoothed to the SHARP1 pixel scale of 0.05" and convolved to the SHARP1 angular resolution of 0.35". To minimize for effects from the saturated nuclear pixels we radially interpolated the flux from the neighboring pixels before convolving and then masked the corresponding pixels in the 0.35" image. To obtain the correct center the position of the northern knot and the position angle given in the header were used. The data was calibrated using the values from McAlary et al. (1983) in ring apertures, since the central pixels were saturated.

### 3. NIR IMAGING SPECTROSCOPY

The  $H$  and  $K$  band spectra (Fig. 1) are fairly flat suggesting effects of extinction, dust emission and maybe an AGN power law continuum may all contribute in addition to the stellar light. This is consistent with the findings from the NIR colors (see section 5.2).

The prominent emission lines in the spectra are the [Fe II] line at  $1.64\mu\text{m}$  in the  $H$  band, and  $\text{H}_2$  lines – especially the  $\text{H}_2$ 1-0 S(1) line at  $2.12\mu\text{m}$  –,  $\text{Br}\gamma$ , and [Si VII] lines in the  $K$  band. Also a number of stellar absorption lines of CO, OH, SiI, NaI and CaI are present. We describe these spectral features in the following sections. Our data agree well with line fluxes and equivalent widths from the literature (Table 2). All line fluxes in this paper were derived from the line maps.

#### 3.1. BLR, CLR and NLR emission lines

In active galaxies emission lines arising at various distances from the central engine can be sub-divided into three main classes. Permitted emission lines with line widths of a few  $10^4$  km/s arise in the BLR with a size of less 1 pc. Forbidden lines with high ionization potential ( $\chi > 100$  eV) arise in the ‘Coronal Line Region’ (CLR) of  $\sim 100$  pc. Permitted and forbidden emission lines with moderate line widths from the NLR can extend over  $\sim 1$  kpc. Emission line maps and fluxes from all three regions are presented in Fig. 2 and Table 3.

Lines from the BLR: The  $\text{Br}\gamma$  line emission in NGC 3227 is mostly unresolved at our resolution of  $1.3''$ . However, at the 10% level of the peak emission, extended flux towards the northeast of the nucleus is apparent. The  $\text{Br}\gamma$  line has a FWHM of  $\sim 650$  km/s. However, due to the triangular line profile (also observed by Vanzi et al. 1998) and our spectral resolution of  $\sim 350$  km/s, it is difficult to determine the exact width. However, the  $\text{Br}\gamma$  FWZI of  $\sim 2400$  km/s is in reasonable agreement with the 2900 km/s found for the variable component of the  $\text{H}\alpha$  line (Salamanca et al. 1994) given the uncertainties.

The peak of the extended  $\text{Br}\gamma$  component coincides with the  $K$  band continuum peak indicating that the BLR is at the position of the continuum. Comparison of the distribution of the molecular gas and its velocity field with the  $VJHK$  colors suggests that the  $K$  band peak and the dynamical center are identical within the uncertainties. This is in contradiction to the result of Arribas & Mediaville (1994) who found an offset between the BLR and the dynamical center. Since parts of the  $\text{H}\alpha$  emission arise in the NLR (see below) and their proposed dynamical center lies in a region with lower  $\text{H}\alpha$  emission (see Figure 5 of Arribas & Mediaville 1994), the velocity field of the  $\text{H}\alpha$  line emission could be dominated by NLR kinematics rather than that of the gravitational potential.

The NLR emission lines: The emitting gas in the NLR of active galaxies has low density ( $10^2$  -  $10^6$ ) and a large spatial extent (10 pc - 1 kpc) which is often cone-like (see review by Wilson 1997). The main excitation mechanism in this region is photo-ionization. The  $\text{Br}\gamma$  emission in NGC 3227 is extended at a very low flux level. The structure and orientation is in agreement with the ioniza-

tion cone as seen in the [O III] line emission (Schmitt & Kinney 1996) and also in the H $\alpha$  map of Arribas & Mediaville (1994). The  $H$  band [Fe II] line emission is still unresolved probably due to the fact that the S/N and spatial resolution is not as high as in the  $K$  band data cube. The width of the [Fe II] line is  $\sim 650$  km/s FWHM typical for NLR lines and comparable to the observed line width of the Br $\gamma$  line. This indicates that the Br $\gamma$  emission is dominated by NLR gas emission. Simpson et al. (1996) suggested that the [Fe II] emission in active galaxies is mainly due to photo-ionization of material with normal ISM abundances by the hard AGN continuum emission. However, a significant fraction ( $\sim 20\%$ ) can still be shock excited. In NGC 3227 the observed  $\frac{[FeII]}{Br\gamma}$  ratio in a 3.6'' aperture is  $2.9 \pm 0.7$  lying between the values found for NGC 1068 and NGC 7469 (Mouri et al. 1990). Excitation by SN remnants (Oliva et al. 1989, Lumsden & Puxley 1995) can be excluded, since in this scenario the [Fe II] and the H $_2$  line emission should spatially coincide. Therefore it seems highly likely that the [Fe II] line is arising from the NLR gas, whereas the H $_2$  emission is probably collisionally excited via shocks (Schinnerer, Eckart & Bertoldi, in prep.).

The CLR emission lines: Due to the high ionization potential ( $\chi > 100$  eV) associated with CLR emission lines high energetic processes are required. If the excitation occurs via collisions, the gas temperature should be about  $T \sim 10^6$ K similar to the corona of the sun. In the case of photo-ionization via the hard AGN continuum, temperatures of only a few  $10^3 - 10^4$ K are needed, however. In NGC 3227 the [Si VI] and marginally the [Al XI] emission lines are detected and spatially unresolved at our resolution and sensitivity. Both lines are located in a wavelength range that is affected by atmospheric absorption features and are close to H $_2$  lines. The same baseline fit was used for the CLR lines and their adjacent H $_2$  lines. Since the CLR lines are spatially unresolved relative to their neighboring continuum whereas the adjacent H $_2$  lines are spatially extended (Fig. 2), we are, therefore confident of their detection. However, due to the different spatial extent of the CLR lines and the diluting H $_2$  lines it is not straight-forward to obtain a corrected CLR line flux.

#### 4. THE STELLAR ABSORPTION LINES

Prominent stellar absorption lines detected in the  $H$  and  $K$  band come from CO, OH, SiI and NaI and arise in the atmosphere of late-type stars. Therefore a noticeable stellar contribution to the continuum is expected. The stellar absorption lines are extended compared to the neighboring continuum with FWHM of 1.5'' and 1.8'' in the  $K$  and  $H$  band, respectively. With a seeing of  $\sim 1.3''$  ( $K$  band) this leads to a size of the nuclear stellar cluster of 0.8'' ( $\approx 70$  pc) after quadratic deconvolution. Line fluxes and equivalent widths are summarized in Table 4. The line maps are shown in Fig. 3. All analysis is done in an aperture of 3.6'' which includes most of the stellar line flux in the corresponding images.

The equivalent widths of SiI ( $1.58 \mu\text{m}$ ), CO 6-3 ( $1.62 \mu\text{m}$ ) and CO 2-0 ( $2.29 \mu\text{m}$ ) can be used to classify the dominating stellar type allowing an estimate of the age of the luminous nuclear stellar cluster. Late-type dwarfs as the main contributors can be excluded due to their low luminosities.

#### 4.1. The spectral class from the SiI and CO 6-3 lines

Origlia et al. (1993), Oliva et al. (1995), Origlia et al. (1997), Oliva & Origlia (1998), Origlia et al. (1999) have analyzed the properties of the SiI (1.58  $\mu\text{m}$ ), CO 6-3 (1.62  $\mu\text{m}$ ) and CO 2-0 (2.29  $\mu\text{m}$ ) lines, and have used the ratios and equivalent widths (EWs) to classify stars as well as stellar populations and clusters. To obtain the equivalent width  $W_\lambda$  the neighboring continuum  $f_\lambda$  is rectified and normalized to unity, the line is then integrated between the limits  $\lambda_1$  and  $\lambda_2$  (as given by Origlia et al. 1993):

$$W_\lambda = \int_{\lambda_1}^{\lambda_2} (1 - f_\lambda) d\lambda \quad (1)$$

The SiI line is only present in stars later than type G4 before it is diluted by the Br14 emission line. The equivalent width depends only on the SiI abundance and therefore the metallicity. The CO lines are observed in stars with  $T_{eff} < 4500$  K and depend on the effective temperature, the surface gravity, the CO abundances (CO 6-3) and the velocity of the microturbulence (CO 2-0).

We can estimate the metallicity from the shape of the CO 6-3 line complex, since it also includes contributions from OH and Ca lines. Oliva & Origlia (1998) and Origlia et al. (1997) show synthesized spectra of this line complex for different metallicities, effective temperatures, and micro-turbulent velocities in the stellar atmospheres.

In NGC 3227 the absorption associated with the CO molecule is significantly stronger than that of the OH line. This indicates that the metallicity in NGC 3227 is at least similar to that inferred for starburst galaxies (Origlia et al 1997) where metallicities of  $[\frac{Fe}{H}] \sim -0.5$  to  $-1.0$  are observed. These calculations have used an upper limit for the effective temperature of 3600 K for the red supergiants, so the metallicities are very likely even higher, since hotter stars need higher metallicities to explain the observed line profiles. Therefore the metallicities inferred for starburst galaxies should be regarded as lower limits (Oliva & Origlia 1998).

The ratio of the equivalent widths of  $\frac{CO\ 6-3}{SiI}$  can be used to estimate the effective temperature of the dominant stellar type in the nuclear stellar cluster of NGC 3227. Since both lines are close in wavelength range, diluting effects such as extinction or non-stellar continuum contributions can be neglected. For NGC 3227 we find within the uncertainties an effective temperature of (3200 - 4200)K for red giants or supergiants suggesting a spectral class of K3 - M6 for giants and K2 - M4 for supergiants (Fig. 4). Comparison of the measured equivalent widths (SiI:  $(1.2 \pm 0.2)\text{\AA}$  and CO 6-3:  $(1.9 \pm 0.1)\text{\AA}$ ) to the expected widths (SiI:  $(4 \pm 1)\text{\AA}$  and CO 6-3:  $(6 \pm 2)\text{\AA}$ ) suggests a stellar contribution of late-type stars to the continuum of  $(30 \pm 10)\%$  in the  $H$  band.



#### 4.2. Further restrictions on the spectral class from the OH line

Meyer et al. (1998) have investigated the dependence of the effective temperature and luminosity class on the  $H$  band stellar absorption lines. They find that the OH line at  $1.689 \mu\text{m}$  is a good indicator for effective temperatures below 4400 K. The OH absorption increases with decreasing effective temperature. The line feature is clearly visible in spectra of red giants and supergiants later than type M0. An additional OH line at  $1.542 \mu\text{m}$  shows a similar behavior.

In NGC 3227 a strong absorption line is present at  $1.548 \mu\text{m}$  which is in agreement with the wavelength of the red-shifted OH line (Fig. 5). This indicates that the stellar light is dominated by cool M stars. The effective temperature is, thus restricted to a much smaller range of  $T_{eff} < 3600$  K (spectral class later than M2) and the stellar contribution of these stars to the total continuum is then about 30% or less. The line emission is extended with respect to the neighboring continuum making the correct identification highly probable. The OH line discussed by Meyer et al. (1998) at  $1.689 \mu\text{m}$  (red-shifted wavelength  $1.696 \mu\text{m}$ ) is not obvious. This is probably due to the fact that the atmospheric correction for that part of the 3D spectrum was not complete. Comparison with an emission spectrum of the earth’s atmosphere shows a number of stronger atmospheric emission lines at this wavelength (Oliva & Origlia 1992, Maihara et al. 1993) compared to the location of the  $1.542 \mu\text{m}$  OH line (red-shifted wavelength  $1.548 \mu\text{m}$ ).

#### 4.3. Possible star formation scenarios for NGC 3227

The equivalent width of the CO 2-0 line depends strongly on the luminosity class of the stars – giant or supergiant (Origlia et al. 1993). Since the slope of the nuclear spectrum suggests a large dilution from non-stellar sources in the  $H$  and  $K$  band, it is not possible to use the observed  $\frac{CO_{6-3}}{CO_{2-0}}$  ratio to obtain the luminosity class. For an effective temperature of 3600 K the expected EW for red giants is  $14 \text{ \AA}$  and  $19 \text{ \AA}$  for red supergiants (Fig. 6). The observed EW of  $(4.0 \pm 0.9) \text{ \AA}$  leads to a stellar continuum contribution from late stars of  $(30 \pm 7)\%$  (red giant case) or  $(20 \pm 5)\%$  (red supergiant case).

Due to the dichotomy in the stellar contribution by red giants or red supergiants to the continuum three scenarios are possible:

(1) The spectrum is dominated by red supergiants. These stars peak around an age of 15 Myr in a starburst (e.g. Schinnerer et al. 1997, Origlia et al. 1999). (2) AGB stars contribute significant to the NIR stellar continuum. The largest number of AGB stars is expected for a starburst with an age of  $\sim 0.5$  Gyr (Lancon 1999). (3) Most of the light is coming from red giants. In this scenario an old stellar population of  $\sim 10$  Gyr – like the bulge population – is present. We investigate these three scenarios in further detail in section 6 using stellar population synthesis and NIR spectral synthesis analysis.

## 5. NIR IMAGING

The high angular resolution NIR data can be used in conjunction with optical HST data to search for structures in the circum-nuclear region (section 5.1). In addition we use these data to estimate the contribution of the AGN and stellar cluster to the NIR continuum via decomposition of the radial surface density profiles and NIR  $JHK$  colors (section 5.2).

### 5.1. The circumnuclear region

A prominent dust lane is visible in the HST image running south-west of the nucleus at a distance of about  $2.5''$ . This structure is best seen in the  $V - H$  and  $V - K$  images (Fig. 8). An additional emission knot is observed about  $5''$  north of the nucleus (Fig. 7). The circumnuclear region exhibits three outstanding components: a ring with  $\sim 0.9''$  radius which is highly likely related to the nuclear molecular gas ring observed in the  $^{12}\text{CO}$  line emission (Schinnerer, Eckart & Tacconi 2000), a  $\sim 1''$  elongated structure in the east-west direction in the  $H - K$  image which is probably be due to the extended  $\text{H}_2$  line emission (Schinnerer, Eckart & Bertoldi in prep., Quillen et al. 2000) and a blue cone north-east of the nucleus which coincides with the ionization cone.

*The ring and the elongated structure:* In the inner  $4''$  a ring segment is very prominent  $\sim 0.9''$  southwest of the nucleus. This ring-like structure surrounds the nucleus entirely at lower magnitudes ( $\sim 3.6^{mag}$  ( $4.0^{mag}$ ) in the  $V - H$  ( $V - K$ ) map). This ring and the nucleus appear to be connected via a  $\sim 1''$  elongated structure seen in the  $H - K$  image (Fig. 8). The ring coincides in radius and orientation with the nuclear molecular gas ring mapped in the  $^{12}\text{CO}$  2-1 line (Schinnerer, Eckart & Tacconi 2000). The elongated structure agrees with the orientation of the NIR  $\text{H}_2$  line emission as observed with 3D (Schinnerer, Eckart & Bertoldi in prep., Quillen et al. 2000). The highly reddened region south-west of the nucleus is likely related to the red-shifted  $^{12}\text{CO}$  emission. This region could be a molecular cloud complex located above the plane of the galaxy (Schinnerer, Eckart & Tacconi 2000).

We checked whether the ring could be an artifact due to misalignment of the HST image versus our NIR data by shifting the images relative to each other in all four directions. The ring structure is a robust feature even if we allow for very large positioning errors of  $0.25''$  (5 pixel). To make sure that the elongated structure is a real feature we made an  $H - K$  color image of the reference star where no such structure is seen. This structure is also seen in the NIR adaptive optics data of Chapman, Morris & Walker (2000).

*The blue cone:* Northeast of the nucleus the colors in the  $V - H$  and  $V - K$  image are bluer by  $\sim 1.1^{mag}$  and  $\sim 1.5^{mag}$ , respectively, compared to the ones southwest of the nucleus. The morphology and position angle of the feature coincides with the ionization cone mapped in its [O III] line (Schmitt & Kinney 1996) suggesting that the blue cone is related to the AGN activity. The colors within the cone are consistent with those of typical E or S0 galaxies (Frogel et al. 1978). This

could indicate that at this position we have a direct view onto the underlying old stellar population. Due to the high-energy AGN radiation in the cone the dust could have been sublimated or removed to allow a direct view onto the stellar disk. The observed difference of  $\sim 1.1^{mag}$  and  $\sim 1.5^{mag}$  in the  $V - H$  and  $V - K$  colors, respectively, might then come from extinguishing material above the disk. Gonzales Delgado & Perez (1997) took optical spectra along various slit positions across the nucleus of NGC 3227. The continuum in the  $V$  band is enhanced north-east of the nucleus as well as the  $H\alpha$  and [O III] line emission up to a radial distance of  $5''$ . Their analysis of the line ratios shows typical values for NLRs.

*Properties of the galaxy disk:* The NIR colors of the disk become redder with radius (see Table 5) suggesting a large contribution of hot dust emission (up to  $\sim 50\%$ ) and an extinction of  $\sim 4^{mag}$  compared with the colors of a typical Sc galaxy (Frogel et al. 1978). This finding is in agreement with the indications for higher extinction found by Barbon et al (1989). They infer a similarly high extinction to explain the observed luminosities of the supernova SN 1983U which occurred about  $18.5''$  west of the nucleus in the disk. This high extinction value for the disk could be due to gas compression because of the interaction with NGC 3226 (Mundell et al. 1995).

*The northern knot:* In all single band images an emission knot about  $5.5''$  north and  $0.9''$  west of the nucleus is apparent. In the HST image this region is unresolved with a FWHM of  $\sim 0.13''$  (Fig. 7). The NIR colors (Table 6) lie within the region occupied by HII regions in the  $JHK$  diagram (Glass & Moorwood 1985). Assuming typical Sc galaxy colors there is evidence for extinction of  $\sim 1.3^{mag}$  and about 20% dust emission ( $T=600K$ ). The measured and dereddened colors of  $V - K=2.5^{mag}$ ,  $J - H=0.6^{mag}$  and  $H - K=0.4^{mag}$  (translates into  $H - K=0.2^{mag}$  if corrected for the dust emission) are consistent with colors expected for K stars (regardless of the luminosity class). In the  $H\alpha$  map of Gonzales Delgado & Perez (1997) no emission is present at this location. However, the region might lie below their detection limit due to its small extent and correspondingly high dilution in seeing-limited images.

## 5.2. The nuclear region

The nucleus of NGC 3227 is compact in all three NIR bands. In the  $J$  and  $H$  band the nucleus is spatially resolved but not in the  $K$  band. This is probably due to the fact that the relative contribution of the nuclear stellar cluster (see section 4) to the nuclear NIR continuum is increasing with shorter wavelength. The  $JHK$  colors suggest a stellar contribution of  $\sim (20 - 50)\%$  extinguished by about 3 magnitudes in a  $0.6''$  aperture. The non-stellar contribution comes very likely from hot dust emission and continuum emission of the AGN itself. In addition an extended component is present which can be identified with the nuclear stellar cluster seen in its stellar absorption lines (see section 4). Smooth-subtracted images (Fig. 7) show no evidence at our achieved sensitivity of  $2 \times 10^{-5}$  Jy/arcsec<sup>2</sup> ( $3\sigma$ ) for the nuclear spiral structure in the inner arcsecond reported by Chapman et al. (2000). Figure 7 also shows the inner  $3''$  of NGC 3227 overlaid with contours of the

PSF in each band.

*The unresolved nuclear (AGN) component:* Comparison of the radial averaged flux density profiles of NGC 3227 and the reference star reveals that most of the  $J$  band source is resolved whereas the nucleus is not resolved in the  $K$  band (Fig. 9). The contribution of the unresolved nuclear component to the overall flux density decreases rapidly with radius (Fig. 9 and 10). The very red nuclear colors of  $J - H = 0.98^{mag}$  and  $H - K = 0.88^{mag}$  in a  $0.6''$  aperture decrease by about  $0.5^{mag}$  at larger radii. The very red colors of the nucleus (compared to the colors of a typical Sc galaxy from Frogel et al. 1978) can be explained via two possible scenarios: (1) A  $\sim 50\%$  contribution of hot dust ( $T=600$  K) together with an extinction of  $A_V = 3^{mag}$  (Fig. 11). (2) The AGN itself contributes to the  $K$  band flux density with  $\sim 50\%$  (with a power law of  $S_\nu \sim \nu^{-1.5}$ ) plus about  $30\%$  from dust emission and about  $20\%$  stellar continuum. The second scenario is consistent with the results of the imaging spectroscopy data (section 3 and 4) and also the modeling results of section 6.

*The resolved nuclear (stellar cluster) component:* The radial surface brightness profiles indicate the presence of a second extended component contributing to the nuclear emission. This component together with the underlying bulge is responsible for at least  $50\%$  of the  $JHK$  flux density at a radius of  $1''$  (after subtraction of the unresolved component, Fig. 9). Decomposing the radial profiles into a unresolved point source representing the AGN and the resolved nuclear stellar cluster with a FWHM of  $\sim 0.9''$  (see section 4) shows that the contribution of the nuclear stellar cluster is decreasing from  $\sim 65\%$  in the  $J$  band to  $40\%$  in the  $K$  band. This is consistent with the values found from the analysis of the 3D data (section 4 and 6). The FWHM for the  $H$  band is in very good agreement with the FWHM of  $0.9''$  found for the nuclear stellar cluster (section 4). The decomposition was more difficult for the  $J$  and  $K$  band, since the sensitivity of the detector in the  $J$  band is lower affecting the proper determination of the brightest peak in the single frame maybe leading to a broadening of the profile. The decomposition in the  $K$  band was hampered by the fact that the stellar contribution is smaller at this wavelength and the PSF did not perfectly match the NGC 3227 data. The extended emission at a  $1''$  radius probably represents the undiluted properties of the nuclear stellar cluster and the underlying bulge population. Its NIR colors of  $J - H = 0.65^{mag}$  and  $H - K = 0.50^{mag}$  can be either explained as a  $\sim 30\%$  contribution due to dust emission (Fig. 11) or as a young stellar population with an extinction of  $(5 - 6)^{mag}$  (see curves in Fig. 8 of Hunt et al. 1997).

The NIR colors in a full  $3.6''$  aperture (as used in section 6 and the appendix) can be either explained by  $\sim 40\%$  dust contribution to the  $K$  band plus a stellar emission which is extinguished by  $1.5^{mag}$ . However, in this case no AGN contribution to the  $H$  and  $J$  band is necessary, in contradiction to the results of the decomposition of the radial surface brightness profiles and the imaging spectroscopic data (section 3). Therefore, the colors have to be explained by a  $\sim 30\%$  dust contribution plus a similar amount of AGN light together with a younger stellar component which is highly extinguished ( $A_V \sim 4-5^{mag}$ ).

## 6. AGE AND DISTRIBUTION OF THE NUCLEAR STELLAR CLUSTER

It is important to estimate the contributions from the nuclear stellar cluster to the total nuclear continuum emission. Winge et al. (1994) have obtained a mean stellar contribution to the nuclear continuum of about  $\sim 40\%$  from observations in the visible. This depends on the age of the stellar population and therefore the modeling of the star formation history. We now look at the three scenarios mentioned in section 4.3 representing different ages using population synthesis and NIR spectral synthesis programs. A short description of these programs together with the estimates of the used parameter is presented in the appendix. The observed values are summarized in Table 7). The aim is to obtain a population dominated by cool M stars consistent with the result of the absorption line analysis (see section 4). To scale the total continuum contribution of M stars accordingly additional non-stellar contributors were added in SPECSYN.

### 6.1. The Model Parameters and the Fitting Procedure

For each scenario we started by fitting the observed contribution of cool stars to the  $K$  band continuum in STARS narrowing the possible model range. Via the stellar flux contribution in the  $K$  band, the  $K$  band luminosity was adjusted for each scenario which resulted in a SFR and enabled us to estimate the stellar mass. In addition the bolometric luminosity  $L_{bol}$ , the Lyman continuum luminosity  $L_{LyC}$ , and the supernova rate  $\nu_{SN}$  were computed for comparison to the observed values (see appendix and Table 7).

The decay time ( $t_{burst}$ ) was set to 100 Gyr for continuous star formation. A decay time of  $t_{burst} = 3$  Myr was used for starbursts. Such a time seems reasonable, as the first supernovae are expected to explode after  $\sim 1$  Myr and to disturb the interstellar medium preventing further star formation. Maiolino et al. (1998) investigated the effect of different decay times on the model parameters. As seen in their Figure 10, the difference in decay time has a strong impact on the parameters connected to high mass stars such as Lyman continuum luminosity or supernova rate whereas the difference in  $L_K/L_{bol}$  is negligible (see also Figure 8b of Genzel et al. (1995) for  $t_{burst} = 5$  Myr). Ideally the decay time  $t_{burst}$  should be treated as a free parameter, however, due to the uncertainties in the observed quantities of  $L_{LyC}$  and  $\nu_{SN}$  no strict constraints can be placed.

In SPECSYN the fit to the spectral slope was done simultaneously in the  $H$  and  $K$  band by adding extinction, dust emission and a contribution of non-thermal AGN emission (see also section 6.2). Since SPECSYN does not include spectra of AGB stars, spectra from M giants were used instead. For mass estimates only stars in the range of  $0.80 M_{\odot}$  ( $\approx K0$  V star) to  $120 M_{\odot}$  are used. Therefore the obtained stellar mass can only be regarded as a lower limit assuming that the IMF is continuous as observed in many cases (see Elmegreen 1999 for an overview).

## 6.2. The Non-Stellar Contributions to the Nuclear NIR Continuum

The discrimination between the three scenarios is independent of the non-stellar components. The best fits to the spectra yielded the same percentage of non-stellar contribution in each case. This can be explained by the general spectral slope of cool M stars, which dominate the stellar light, and is similar for all three scenarios.

The following procedure was adopted: (1) In the  $H$  band the AGN power law contribution to the observed spectrum was adjusted by matching the depth of the stellar absorption features. (2) The value of the extinction was derived by matching the slope of the observed  $H$  band spectrum. (3) The  $\lambda 2.29\mu\text{m}$  CO bandheads were used together with the  $K$  band spectral slope to define the dust temperature as well as the dust contribution. (4) The AGN power law contribution was checked and re-adjusted to fit the observed  $H$  and  $K$  band spectrum. This method is relatively robust, since the AGN power law contribution and the extinction are derived almost independent of each other, as they affect the  $H$  band spectrum very differently. By fitting the  $K$  band spectrum the only free parameter is then the contribution of hot dust emission which can be treated independently. Changes of  $\sim 100$  K in the dust temperature give already no longer satisfying fits to the spectrum despite varying the relative contribution of the dust emission.

For all three scenarios the modeling resulted in similar amounts for the stellar contribution to the total continuum within the given uncertainties (Fig. 12). The values for the hot dust emission ( $\sim 25\%$ ), the AGN contribution ( $\sim 35\%$ ) and the extinction ( $A_V \sim 5^{mag}$ ) are in agreement with those derived from the  $JHK$  colors (see section 5.2). In the  $H$  band about 65% and in the  $K$  band about 40% of the continuum are due to stellar light. In addition we find an extinction of  $A_V \sim (4-5)^{mag}$ . The difference is due to the SEDs of the different contributing components. In the case of NGC 3227 this means that the  $H$  band is less affected/contaminated by emission associated with the AGN. Although, the contribution from the power law component is larger than in the  $K$  band due to the low spectral index, the contribution of the hot dust emission is much larger in the  $K$  band. Changes in  $\alpha$  for the AGN power law contribution have no relevant effects on the fitting in the range of -1.1 to -0.6, since the slope is relative shallow. We adopted  $\alpha = -0.9$ , as this is consistent with the slope observed in the varying optical continuum of NGC 3227 (Winge et al. 1995). The derived dust temperature is of the order of 950 K, in agreement with findings from Oliva et al. (1995) who found similarly high dust temperatures in their Seyfert sample. As outlined above, the derived dust temperature (plus the relative contribution of the dust emission) is very sensitive to the longer wavelength range of the  $K$  band. Assuming, that the derived values for the extinction and AGN power law contribution from the  $H$  band fit are correct, this leaves only a small range of about  $\pm 70$  K for the dust temperature. However, it is very likely that two dust emitting components are present one associated with the AGN and the other with the stellar cluster.

### 6.3. The AGB Scenario: 0.5 Gyr old Starburst

This scenario can be discriminated from the other two using the spectra, colors, spectral lines and the results from the population and NIR spectral synthesis.

The spectral slope: Comparison with the composite spectra of Lancon (1999) shows that a 200 Myr stellar cluster that contains only C-rich AGB stars shows a prominent sharp absorption edge due to the  $C_2 \lambda 1.77 \mu\text{m}$  line. Such a prominent feature is not observed in the spectra of NGC 3227. Since the line is shifted at the band edge where the atmospheric calibration is poorer, this possibility can not be completely excluded. However, the overall spectral slope is not in agreement with the AGB spectra of Lancon (1999).

In the case of a 200 Myr old stellar cluster dominated by O-rich AGB stars, the spectrum is dominated by deep  $H_2O$  absorptions between the  $H$  and  $K$  band which affect the  $H$  band more than the  $K$  band. The continuum drops significantly towards the band edges. Such a behavior is not obvious in the  $H$  and  $K$  band spectrum of NGC 3227. This indicates that O-rich AGB stars are not the dominant spectral type. The  $H$  and  $K$  band spectrum obtained by Vanzi et al. (1998) also show no drop in flux at the band edges. Since no synthetic spectrum showing a mixture of C- and O-rich AGB stars or showing AGB stars at different age is given by Lancon (1999), this scenario can not completely be excluded from the spectral slope alone, however.

The colors: As shown by Lancon (1999) the  $V - K$  and  $J - K$  colors can be used to discriminate AGB dominated populations from older (giant dominated) populations. The pure colors of the nuclear stellar cluster of NGC 3227 can be estimated from the radial averages (Fig. 10) at a radius of  $\sim 1''$  to minimize contamination from the AGN. As shown in section 5.2, the  $JHK$  colors (of the extended emission in Fig. 11) can be explained either by a young cluster with strong extinction or 30% dust emission in addition to an underlying bulge component with typical Sc colors (Frogel et al. 1978). However, the underlying bulge component might already completely dominated the colors as suggested by the radial decomposition (Fig. 9). The measured  $J - K$  color of  $\approx 1.15^{mag}$  is similar to the expected value of  $(0.9 - 1.0)^{mag}$  during the AGB phase (Lancon 1999). The observed  $V - K$  color is  $\approx 4.6^{mag}$ . However, the interpretation is complicated by the fact that a significant fraction of the  $V$  band flux density comes from the NLR lines. This is quite obvious in the  $V - K$  color map where the ionization cone is prominent in bluer colors. To take this into account, one has to decrease the  $V$  band flux and therefore increase the  $V - K$  color. On the other hand the  $V$  band flux has to be increased due to the observed extinction (see section 5.2). This makes it possible that the AGB phase  $V - K$  colors of about  $2.5^{mag}$  (Lancon 1999) can be matched. The analysis is, however, hampered by the fact that the exact contribution of the nuclear stellar cluster to all the individual bands is uncertain.

MgI/AlI at  $2.11 \mu\text{m}$ : The  $K$  band spectrum of NGC 3227 shows indications for absorption lines from MgI/AlI at  $2.11 \mu\text{m}$  (Fig. 5). In the corresponding line map (Fig. 3) the 50% contour of the absorption is extended with respect to the neighboring continuum in agreement with the other

observed stellar lines. In the spectra of three AGB stars (two C-rich, one O-rich) from Wallace & Hinkle (1997) no MgI/AlI absorption feature is present. The comparison of the lower limit of the equivalent width (value minus  $3\sigma$  value) to the expected value of an M star of  $4.9 \text{ \AA}$  suggests that at least about 15% of the total continuum can be due to M stars. Since about 40% of the  $K$  band continuum is of stellar origin, these 15% translate then into about 40% of the stellar light coming from M stars and not AGB stars. This result is just in agreement with the models for the (peak) AGB phase where up to 50% of the  $K$  band continuum can be due to AGB stars (Lançon 1999). However, since the EW of MgI/AlI is probably higher the contribution from AGB stars is lower indicating that the nuclear stellar light is not completely dominated by AGB stars.

Population and NIR spectral synthesis: Since there is an insufficient number of spectra for AGB stars available in the literature, we approximated the AGB spectra in SPECSYN with spectra from cool M stars (which should give a reasonable agreement in the spectral slope). The relevant numbers of the population synthesis are given in Table 7. The percentage of the M stars to the  $K$  band light is at the lower limit of the observed value. The present-day stellar mass is only a third of the dynamical mass in the inner  $3.6''$ . The estimated black hole mass is about  $4 \times 10^7 M_{\odot}$  (Ho 1998) and the molecular gas mass is about  $5 \times 10^7 M_{\odot}$  (Schinnerer, Eckart & Tacconi 2000). This indicates that there must be an additional older ( $> 1 \text{ Gyr}$ ) stellar population which contributes little to the observed light but a lot to the mass. To verify our spectral synthesis we fitted the spectrum of the Mira star  $\chi \text{ Cyg}$  (Wallace & Hinkle 1997) plus an additional flat continuum to the  $K$  band spectrum of NGC 3227. To obtain a reasonable fit in the spectral slope (Fig. 1) a non-stellar continuum of about 70% is needed in agreement with the results of the spectral synthesis.

In conclusion, most of the evidence does not favor the AGB phase and therefore an age of  $\sim 5 \times 10^8 \text{ yr}$ . However, despite the remaining uncertainty in addition to the mapped nuclear stellar cluster at least a second much older stellar population must be present.

#### 6.4. The RG Scenario: Old Stellar Cluster

The light of an old ( $\sim 10^{10} \text{ yr}$ ) starburst would be dominated by late type main-sequence stars. However, such a scenario would require that no molecular gas could have recently reached the nuclear region and be transformed into new stars. This seems unlikely given the large molecular gas concentrations observed close to the center (Schinnerer, Eckart & Tacconi 2000) and the observed nuclear activity (AGN). Therefore we assume a large age (10 Gyr) with constant star formation which leads to a giant dominated stellar population. Table 7 summarizes the fit values. The relative contribution from M stars in the  $K$  band is smaller than those deduced from the stellar absorption lines. In addition to M stars, K stars contribute about 30% to the stellar continuum in the  $K$  band. The resulting spectral fit (Fig. 13) is not as good as in the RSG case for the CO bandheads longward of  $2.30 \mu\text{m}$ . A small change in the dust temperature can, however, minimize this effect. The present-day stellar mass which is a lower limit due to the cut-off in the IMF is



close to the obtained dynamical mass, if one accounts for the neglected low-mass stars. However, in this scenario the total observed (spatially unresolved)  $\text{Br}\gamma$  emission could be explained by the nuclear stellar cluster. Since, the stellar absorption lines are spatially extended whereas the  $\text{Br}\gamma$  line emission is not, this indicates different origins for the two lines. Even including extinction of the  $\text{Br}\gamma$  line flux can not solve this discrepancy in the spatial distribution. Therefore, continuous star formation over the last 10 Gyr seems highly unlikely.

### 6.5. The RSG Scenario: Young $\sim$ 25 Myr Starburst

The contribution of M-type RSG stars to the stellar  $K$  band light is largest at an age of 25 Myr with about 55% contribution. In order to explore the age range there RSG stars dominate the NIR light, we computed the model values at three different ages (15 Myr, 25 Myr, and 50 Myr; see Table 7). The resulting spectral fit for an age of 25 Myr is presented in Fig. 14. As in the case of the AGB phase (section 6.3) the present-day stellar mass is only a fraction of the total dynamical mass, again, indicating that besides that young luminous population at least one much older and less luminous population must be present at the center of NGC 3227 in addition to the black hole and the molecular gas. The Lyman continuum luminosity  $L_{LyC}$  for this burst is considerable low for burst ages of 25 Myr and larger. Since the bolometric luminosity  $L_{bol}$  and the supernova rate  $\nu_{SN}$  are similar to the observed values for an age of 25 Myr, this indicates an age even larger than 25 Myr, if the AGN is contributing to these quantities. However, to still match the relative contribution of the M stars to the NIR continuum, a burst age below 50 Myr is favored.

### 6.6. Further Support for the RSG Scenario from Optical Absorption Lines

Optical observations of the nuclear region in NGC 3227 also point towards a younger stellar population of RSG stars. In the optical bands the CaII triplet at  $\lambda 8498\text{\AA}$ ,  $8542\text{\AA}$ ,  $8662\text{\AA}$  and the MgI  $b$  line at  $\lambda 5171\text{\AA}$  can be used as a diagnostic line ratio. The CaII lines arise in the atmospheres of late type stars and show a similar dependency on the luminosity class as seen for the  $\lambda 2.29\mu\text{m}$  CO 2-0 line (e.g. Terlevich et al. 1990). Different measurements of the MgI  $b$  line towards the nucleus of NGC 3227 indicate a stellar contribution of 17% - 30% (Terlevich et al. 1990, Malkan & Filippenko 1983, Winge et al. 1995) whereas measurements of the CaII triplet suggest a stellar contribution of about 60% (Terlevich et al. 1990). This large discrepancy can be explained if the CaII lines arise in the atmospheres of RSG stars and not RG stars.

In the spectra of Nelson & Wittle (1995) the CaII triplet is clearly detected whereas the MgI  $b$  line is only weak. Dilution of the MgI  $b$  line by the neighboring emission lines of [Fe VII] and [Fe VI] can be excluded, since the equivalent width in the high spectral resolution spectrum of Malkan & Filippenko (1983) is small as well. The small EW of the stellar absorption line of FeI  $\lambda 5268\text{\AA}$  which shows the same strength as the MgI  $b$  line in starburst galaxies (Malkan & Filippenko 1983) is consistent with this finding.

The varying AGN continuum can not account for the difference in stellar contribution derived from both lines: The continuum varies with a period of  $\sim 17$  d (Winge et al. 1995, Salamanca et al. 1994). However, the amplitude at 5200 Å and 8500 Å is only about 10% (s. Fig. 1 of Winge et al. 1995) allowing not for such a large difference in the stellar contribution. The difference still persists if the CaII triplet is observed during the AGN minimum and the MgI *b* line during AGN maximum. Salamanca et al. (1994) measured the EW of MgI *b* in the minimum and maximum and their value is in agreement with that of Winge et al. (1995). This confirms that the CaII line is indeed stronger relative to the MgI *b*, thus suggesting a significant contribution of RSG stars to the stellar light.

Alternatively, different wavelength dependent extinction towards the nuclear stellar cluster could explain the discrepancy. However, this would imply different AGN contributions at the visible and red wavelength range in contradiction to the observed flat slope of the variable AGN continuum at these wavelengths (Winge et al. 1995).

## 7. SUMMARY AND CONCLUSIONS

In the NIR continuum of NGC 3227 we find besides the unresolved AGN component a stellar nuclear cluster with a FWHM of  $\sim 70$  pc. At least two stellar populations with different ages are observed in the nucleus of NGC 3227. Continuous star formation can be ruled out implying that the nuclear star formation takes place in episodes. This is in agreement with the large reservoir of molecular material at a radial distance of  $\sim 100$  pc from the nucleus and also associated with the HII regions in the inner 1 kpc. Since the gas dynamics in the inner 1 kpc are complex (Schinnerer, Eckart & Tacconi 2000), the probability that gas will become instable and form stars is quite high. We find more evidence for a nuclear stellar cluster with an age of 25 to 50 Myr when most of the NIR stellar light comes from RSG stars rather than an age of  $\sim 5 \times 10^8$  yr where the NIR light is dominated by AGB stars.

- The nuclear stellar light in the *H* and *K* band is dominated by emission from very cool evolved stars. The analysis of the stellar absorption lines indicates M giants or supergiants as the dominant stellar type. From our population and spectral synthesis we can rule out constant star formation over the past 10 Gyr which could produce an M giant dominated population.
- Investigation of the other two likely scenarios (RSG phase with an age of  $\sim 25$  Myr or AGB phase with an age of  $5 \times 10^8$  yr) shows that none can be ruled out completely. However, supporting evidence for the RSG scenario is found from optical observations which point towards a large contribution of RSG stars to the stellar light. In the RSG scenario the nuclear stellar cluster produces most of the MIR/FIR emission, a substantial fraction of the H recombination line fluxes and the radio flux. This implies that a considerable amount of the nuclear luminosity is coming from the starburst and not the AGN component.

- Although the AGB scenario can not be excluded, the observed parameters are at the uncertainty limits for this model. Due to the different spatial resolution of the imaging and imaging spectroscopic data a more detailed analysis is not possible. In addition it seems unlikely that no nuclear star formation has occurred in the last  $10^8$  yr given the large molecular gas reservoir close to the inner  $3.6''$ . To evaluate this further data at higher S/N and with a larger coverage in the wavelength range are needed.
- It is interesting to note that in the case of either the RSG or AGB scenario the mapped nuclear stellar cluster accounts for only  $\sim 15\%$  of the dynamical mass in the inner  $3.6''$ . As the mass contribution of the black hole and the molecular gas is of the same order, this implies that a least another stellar population exists which is much older and less luminous. Such a scenario is similar to the center of our own galaxy where stars from several star forming episodes are observed (Krabbe et al. 1995). This is also consistent with the findings of Tecza et al. (2000) for NGC 6240. In a possible scenario the star formation and AGN activity might go through cycles of high and low activity depending on whether the nuclear starburst is providing fuel for the AGN or not.
- The stellar contribution to the continuum emission is largest in the  $H$  band with  $65\%$ , whereas the fraction of the stellar light is only  $\sim 40\%$  in the optical and  $K$  band. The results of the spectral synthesis are in agreement with the findings of the decomposition of the NIR radial flux density profiles. The extended component shows a significant extinction of  $A_V \sim (4 - 5)^{mag}$  assuming young stars (Hunt et al. 1997). The nuclear AGN component ( $0.5''$ ) suggests an extinction of  $\sim 3^{mag}$  as well. However, the analysis of the  $JHK$  colors is strongly affected by the co-existence of an old not luminous and a young stellar population and the AGN contributions in the inner 500 pc.
- In our high angular resolution NIR data the nucleus is slightly resolved at  $J$  and  $H$  band, clearly showing the nuclear stellar cluster as an additional extended component.  $VJHK$  color images show the structure of the ionization cone as well as enhanced extinction south-west of the nucleus.

We would like to thank the MPE 3D team (N. Thatte, L.J. Tacconi-Garman, H. Kroker, S. Anders, R. Maiolino, J. Gallimore) for obtaining the data and the staff of the WHT and the Calar Alto 3.5 m for their support. The NTT staff was very helpful during the SHARP observations. For fruitful discussions we like to thank R. Genzel. L. Armus' comments helped to improve and clarify the manuscript. We thank H. Schmitt for kindly providing us with the HST [O III] map of NGC 3227.

## APPENDIX

## A. STELLAR POPULATION AND NIR SPECTRAL SYNTHESIS

Here we give a short description of the stellar population synthesis code STARS together with a discussion of general caveats. We also outline the structure of the NIR spectral synthesis code SPECSYN. The observational parameters which are used for modeling are derived in this section as well.

### A.1. Population synthesis

The aim of the population synthesis is to obtain a model reflecting the star formation history of the galaxy. Theoretical stellar evolutionary tracks are used in conjunction with an initial stellar mass function (IMF). It is assumed that stars with  $M > 8 M_{\odot}$  explode as supernovae after their supergiant phase. Some also experience the Wolf-Rayet phase during which strong stellar winds influence the evolution of the star. Stars with masses between  $8 M_{\odot}$  and  $30 M_{\odot}$  become red supergiants which have strong contributions in the NIR due to their low effective temperatures. Stars with masses below  $8 M_{\odot}$  evolve into red giants where stars with masses between  $2 M_{\odot}$  and  $7 M_{\odot}$  reach the asymptotic giant branch. At this point they show a strong luminosity increase at very low effective temperatures (AGB phase), and then evolve to planetary nebulae.

*High-mass stars:* The evolutionary tracks for high-mass stars have uncertainties at different evolutionary stages regarding the time-span and the related physical parameters such as effective temperatures, luminosity and mass loss. The rotation of massive stars can, e.g., reduce their mass loss rate and therefore change their lifetime on the main sequence (Langer 1998). Talon et al. (1997) have investigated the influence of the rotation velocity for a  $12 M_{\odot}$  star. At the same effective temperature the star showed a higher luminosity at high rotation velocities (of 300 km/s). Therefore knowledge of the mean rotation velocity is necessary to calculate the stellar evolutionary tracks, since the mass loss during the main sequence influences the evolution of the star at later stages. The evolutionary tracks for stars with  $15 M_{\odot} < M < 30 M_{\odot}$  never reach low effective temperatures of  $T \sim 3000$  K during the red supergiant phase, although such stars are observed (Langer & Maeder 1995). However, effective temperatures of about 3500 K equivalent of early M supergiants are reached. The depths of the prominent NIR absorption lines are relatively similar for M supergiants as well as the NIR spectral slope compared to the hotter stars. Therefore the effects on the NIR spectral synthesis are sufficiently small. Only the difference in luminosity can affect the population synthesis by underestimating both bolometric and  $K$  band luminosity. However, again the scatter within the M supergiants is reasonably small, if the ratio of  $L_K/L_{bol}$  is considered for M supergiants (ranging from 0.11 (M0I) to 0.15 (M5I)). As discussed in section 4 the metallicity derived for the nuclear stellar cluster in NGC 3227 is close to solar, thus justifying to use the evolutionary tracks for solar metallicity which give reasonable results for the red supergiant phase (Origlia & Oliva 2000). Understanding the evolution during the Wolf-Rayet phase is also in progress, and models include effects such as line blanketing (e.g. adding atomic lines like O,

Gräfener et al. 1998) and clumping in the stellar winds (Nugis et al. 1998). These effects influence the mass loss and therefore the lifetime of a Wolf-Rayet star. Since the ages relevant for our analysis are considerably longer than the lifetimes of WR stars, this effect can be neglected.

Binary stars: Van Bever & Vanbeveren (1998) have investigated the effect of binary stars on the evolution of star forming regions via number population synthesis calculations. The mass transfer in close binaries, so called 'accretion stars', can make these stars appear in the stellar population as O type stars at a time at which normal O type stars would have already evolved away from the main sequence. This is a natural explanation for the 'blue stragglers' found in a number of stellar clusters. In this case the star forming region is older, as suggested by the appearance of the accretion stars. However, the number of accretion stars depends strongly on the abundance of binary stars and the mass transfer via the Lagrange point  $L_1$  with 'Roche lobe overflow'. Since the correct handling of the binary star evolution is not clear, this effect is not taken into account by STARS.

Low-mass stars: In the evolutionary tracks of low-mass stars the less understood phase is the asymptotic giant branch phase (AGB-phase). AGB stars appear at a similar location as red giants in the HR-diagram, and the progenitor stars are more massive. This means that these stars reach their location in the HRD much earlier. Modeling of the AGB phase at the tip of the giant branch just before the transition to a planetary nebula is difficult, since the stars change their luminosity, effective temperature and chemical composition. NIR observations show that AGB stars can change their effective temperatures by 500 K and their luminosities by 25% within short time-scales (Lancon 1999). Spectra of AGB stars are characterized by deep molecular absorption bands of  $H_2O$  (O-rich AGB stars) and  $C_2$  (C-rich AGB stars) (Lancon 1999 and references therein).

Lancon (1999) investigates the influence of AGB stars on the observable parameters of stellar populations using the population synthesis code PEGASE (Fioc & Rocca-Volmerange 1997). She compares a synthetic spectrum of a 4 Gyr old giant-dominated population to a 200 Myr old (C- or O-rich) AGB stars dominated population. The continuum clearly shows the strong molecular absorption features of the AGB stars in the later case. About 0.3 -1.5 Gyr after an intense burst of star formation the contribution of AGB stars to the total emission of the stellar population is the largest (Lancon 1999), and can be as high as about 50% to the total  $K$  band light.

The stellar evolutionary tracks used by STARS have been extended to the TP-AGB phase using the models of Bedijn (1988) similar to the method of Lançon & Rocca-Volmerange (1996). A detailed description is given by Schreiber (1998).

The initial mass function (IMF): The initial mass function (IMF) describes the number of stars formed per mass interval. For our calculations with STARS we have used a power law ( $\sim M^{-\alpha}$ ) with a typical value of  $\alpha = -2.35$  for stars between about  $0.80 M_{\odot}$  and  $120 M_{\odot}$  (Salpeter 1955, Leitherer 1996, review by Elmegreen 1999). For lower masses the IMF shows a flatter slope (Scalo 1986). The analysis is complicated by the fact that the emission from low-mass stars is weak in the NIR and therefore harder to analyze.

### A.2. The NIR spectral synthesis

We test the results from our population synthesis analysis with the NIR spectral synthesis program SPECSYN by including the contribution from non-stellar continuum sources to the NIR light. SPECSYN uses the HR-diagrams to synthesize spectra by combining standard stellar spectra from the literature at the instrumental resolution of 3D. A detailed description of SPECSYN is given in the appendix of Schinnerer et al. (1997).

For the purpose of this paper SPECSYN has been expanded to also synthesize  $H$  band spectra. We have implemented the possibility to add AGN emission as a power law. The coverage in the  $H$  band is achieved with the stellar library from Meyer et al. (1998) and in the  $K$  band with the library from Wallace & Hinkle (1997). The advantage is that all spectra have the same wavelength coverage and were obtained with the same instrument representing a homogeneous data set. The HR-diagram coverage is done in analogy to Schinnerer et al. (1997). The influences of the various parameters on the  $H$  and  $K$  band spectra are shown in Fig. 15, and the parameters are summarized in Table 8.

*The non-stellar contributors:* Extinction, dust emission or AGN continuum emission can be a possible source of dilution to the stellar continuum. The non-stellar contributors are included as percentages to the total flux at the central wavelength in the  $H$  and/or  $K$  band. In the case of simultaneous spectral synthesis the  $K$  band percentage values are given and interpolated to values for the  $H$  band. Extinction and dust emission are treated as given by Schinnerer et al. (1997). The AGN is not only heating the surrounding dust (leading to thermal emission in the MIR/FIR) but also has a strong continuum in the UV and optical range. For the AGN continuum emission, we assume a power law of the form  $I_{AGN}(\lambda) \sim \lambda^\alpha$ , where  $\alpha$  is a free parameter with typical values of -0.8 for the wavelength range relevant here. Malkan & Filippenko (1983) and Edelson & Malkan (1986) find values for  $\alpha$  between -0.9 and -0.64 by fitting the non-stellar continuum of a sample of Seyfert galaxies. As mentioned by the authors this slope is very similar to quasars. However, it is hard to isolate the pure AGN contribution, since it consist of at least two emission components: The Balmer continuum and the UV black body ( $T > 26000\text{K}$ ) (Edelson & Malkan 1986). Sanders et al. (1989) speculate that the different components might arise at different distances from the central engine: the UV is dominated by light from the accretion disk, whereas the IR is dominated by light from the outer parts of the disk at radii of 0.1 pc to 1 kpc and is emitted by dust in the host galaxy.

### A.3. The observational parameters

The *bolometric luminosity* is assumed to be similar to the IR luminosity, since most of the UV energy is transformed to IR wavelengths due to the photo-electric heat mechanism (Tielens & Hollenbach 1985). The IR luminosity can be derived using the IRAS fluxes and the equation given by Sanders & Mirabel (1996). From the IRAS fluxes at  $12\mu\text{m}$  (0.62 Jy),  $25\mu\text{m}$  (1.75 Jy),  $60\mu\text{m}$  (7.84 Jy) and  $100\mu\text{m}$  (16.93 Jy) and using

$$L_{bol}[L_{\odot}] = 5.617 \times 10^5 \times D[Mpc]^2 \times (13.48 f_{12\mu m}[Jy] + 5.16 f_{25\mu m}[Jy] + 2.56 f_{60\mu m}[Jy] + f_{100\mu m}[Jy])$$

the observed bolometric luminosity is  $\sim 9.3 \times 10^9 L_{\odot}$ . The 10  $\mu m$  map of Bushouse, Telesco & Werner (1998) shows an unresolved source in the inner 400 pc of NGC 3227. Their 100  $\mu m$  map shows that the total emission is associated with NGC 3227. This suggests that most, if not all, of the IRAS fluxes are coming from the inner 400 pc and this is a good approximation for the nuclear bolometric luminosity, neglecting high-energy AGN contributions. The estimated derived bolometric luminosity can, however, still have AGN contributions and is therefore regarded as an upper limit.

The *K band luminosity* comes from cool and therefore evolved stars. We use the definition

$$L_K[L_{\odot}] = 1.16 \times 10^4 \times D[Mpc]^2 \times S_K[mJy]$$

given by Genzel et al. (1995) with a *K* band width of 0.6  $\mu m$ .

The *Lyman continuum luminosity* is associated with the HII regions around hot stars, giving a measure for the contribution from young, hot stars. Using the observed Br $\gamma$  line flux the Lyman continuum luminosity can be estimated via

$$L_{Ly\alpha}[L_{\odot}] = 5.37 \times 10^{19} \times F_{Br\gamma}[ergs^{-1}cm^{-2}] \times D[Mpc]^2$$

As discussed in section 3.1 most of the nuclear Br $\gamma$  line emission in NGC 3227 is associated with the BLR and NLR. Only a small percentage of the Br $\gamma$  line flux comes from HII regions around hot stars.

To estimate the *supernova rate* we use the empirical relation given by Condon (1992). Huang et al (1994) found a similar number by direct comparison of the SN numbers to the radio emission in the starburst galaxy M 82. To obtain  $\nu_{SN}$  we used the total nuclear 5 GHz flux density of Mundell et al. (1995b) and

$$\nu_{SN}[yr^{-1}] = 3.3 \times 10^{-6} \times S_{5GHz}[mJy] \times D[Mpc]^2$$

Since the 5 GHz flux density of Mundell et al. (1995b) might have contributions from the AGN, the derived supernova rate is an upper limit. All values are summarized in Table 7.

## References

- Arribas, S., Mediavilla, E., 1994, *Ap. J.*, 437, 149.
- Barbon, R., Ciatti, F., Iijima, T., Rosino, L., 1989, *Astron. Astrophys.*, 214, 131.
- Barvainis, R., 1990, *Ap. J.*, 353, 419.
- Bedijn, P.J., 1998, *Astron. Astrophys.*, 205, 105.
- Bushouse, H.A., Telesco, C.M., Werner, M.W., 1998, *A. J.*, 115, 938.
- Calzetti, D., 1997, *A. J.*, 113, 162.
- Christou, J.C., 1991, *Exp. Astro.*, 2, 27
- Colina, L., Pérez-Olea, D.E., 1995, *M.N.R.A.S.*, 277, 845.
- Condon, J. J., 1992, *Ann. Rev. Astron. Astrophys.*, 30, 575.
- Dallier, R., Boisson, C., Joly, M., 1996, *Astron. Astrophys. Suppl.*, 116, 239.
- De Robertis, M.M., Hayhoe, K., Yee, H.K.C., 1998, *Ap. J. Supp.*, 115, 163.
- De Vaucouleurs, G, de Vaucouleurs, A., Corwin, H., Buta, R., Paturel, G., Fougué, P., 1991, *Third Reference Catalogue of Bright Galaxies*, Berlin, Springer-Verlag)
- Devereux, N.A., 1989, *Ap. J.*, 346, 126.
- Eckart, A., van der Werf, P.P., Hofmann, R., Harris, A.I., 1994, *Ap. J.*, 424, 627.
- Edelson, R.A., Malkan, M.A., 1986, *Ap. J.*, 308, 59.
- Elmegreen, B.G., 1999, 'Unsolved Problems in Stellar Evolution', ed. M. Livio, Cambridge Univ. Press, in press
- Fioc, M., Rocca-Volmerange, B., 1997, *Astron. Astrophys.*, 326, 950.
- Fischer, J., Geballe, T.R., Smith, H.A., Simon, M., Storey, J.W.V., 1987, *Ap. J.*, 320, 667.
- Förster Schreiber, N.M., 2000, *astro-ph/0007324*
- Forbes, D.A., Ward, M.J., 1993, *Ap. J.*, 416, 150.
- Frogel, J.A., Persson, S.E., Aaronson, M., Matthews, K., 1978, *Ap. J.*, 220, 75.
- Garcia, A.M., 1993, *Astron. Astrophys. Suppl.*, 100, 47.
- Genzel, R., Weitzel, L., Tacconi-Garman, Blietz, M., Krabbe, A., Lutz, D., Sternberg, A., 1995, *Ap. J.*, 444, 129.
- Glass, I.S., Moorwood, A.F.M., 1985, *M.N.R.A.S.*, 214, 429.



- González Delgado, R.M., Perez, E., 1997, M.N.R.A.S., 284, 931.
- Gräfener, G., Hamann, W.-R., Hillier, D.J., Koesterke, L., 1998, Astron. Astrophys., 329, 190.
- Ho, L.C., 1998, Invited review to "Observational Evidence for Black Holes in the Universe", ed. S.K. Chakrabarti (Dordrecht: Kluwer), in press)
- Hofmann, R., Brandl, B., Eckart, A., Eisenhauer, F., Tacconi-Garman, L.E., 1995, SPIE-Conference, Orlando
- Huang, Z.P., Thuan, T.X., Chevalier, R.A., Condon, J.J., Yin, Q.F., 1994, Ap. J., 424, 114.
- Hunt, L.K., Malkan, M.A., Salvati, M., Mandolesi, N., Palazzi, E., Wade, R., 1997, Ap. J. Supp., 108, 229.
- Kleinmann, S.G., Hall, D.N.B., 1986, Ap. J. Supp., 62, 501.
- Kotilainen, J.K., Ward, M.J., Boisson, C., De Poy, D.L., Bryant, L.R., Smith, M.G., 1992, M.N.R.A.S., 256, 125.
- Krabbe, A., Sternberg, A., and Genzel, R., 1994, Ap. J., 425, 72.
- Lançon, A., 1999, 'Asymptotic Giant Branch Stars', IAU Symposium 191, in press, astro-ph9810474
- Langer, N., 1998, Astron. Astrophys., 329, 551.
- Langer, N., Maeder, A., 1995, Astron. Astrophys., 295, 685.
- Leitherer, C., 1996, in ASP.conf. series Vol.98, p. 373.
- Lord, S., 1992, NASA Technical Memorandum 103957, Ames Research Center, Moffett Field, CA
- Lumsden, S.L., Puxley, P.J., 1995, M.N.R.A.S., 276, 723.
- Maihara, T., Iwamuro, F., Yamashita, T., Hall, D.N.B., Cowie, L.L., Tokunaga, A.T., Pickles, A., 1993, PASP105940
- Maiolino, R., Krabbe, A., Thatte, N., Genzel, R., 1998, Ap. J., 493, 650.
- Malkan, M.A., 1988, Adv. Space Res., Vol. 8, No. 2-3, 49
- Malkan, M.A., Filippenko, A.V., 1983, Ap. J., 275, 477.
- Malkan, M.A., Gorjian, V., Tam, R., 1998, Ap. J. Supp., 117, 25.
- McAlary, C.W., McLaren, R.A., Gonegal, R.J., 1983, Ap. J. Supp., 52, 341.
- Meyer, M.R., Edwards, S., Hinkle, K.H., Strom, S.E., 1998, Ap. J., 508, 397.
- Mouri, H., Nishida, M., Taniguuchi, Y., Kawara, K., 1990, Ap. J., 360, 55.
- Mulchaey, J.S., Regan, M.W., Kundu, A., 1997, Ap. J. Supp., 110, 229.

- Mundell, C.G., Holloway, A.J., Pedlar, A., Meaburn, J., Kukula, M.J., Axon, D.J., 1995a, M.N.R.A.S., 275, 67.
- Mundell, C.G., Pedlar, A., Axon, D.J., Meaburn, J., Unger, S.W., 1995b, M.N.R.A.S., 277, 641.
- Nelson, C.H., Whittle, M., 1995, Ap. J. Supp., 99, 67.
- Norman, C., Scoville, N., 1988, Ap. J., 332, 124.
- Nugis, T., Crowther, P.A., Willis, A.J., 1998, Astron. Astrophys., 333, 956.
- Oliva, E., Moorwood, A.F.M., 1990, Ap. J. (Letters), 348, L5.
- Oliva, E., Moorwood, A.F.M., Danziger, I.J., 1989, Astron. Astrophys., 214, 307.
- Oliva, E., Moorwood, A.F.M., Danziger, I.J., 1990, Astron. Astrophys., 240, 453.
- Oliva, E., Origlia, L., 1992, Astron. Astrophys., 254, 466.
- Oliva, E., Origlia, L., 1998, Astron. Astrophys., 332, 46.
- Oliva, E., Origlia, L., Kotilainen, J.K., Moorwood, A.F.M., 1995, Astron. Astrophys., 301, 55.
- Origlia, L., Ferraro, F.R., Fusi Pecci, F., Oliva, E., 1997, Astron. Astrophys., 321, 859.
- Origlia, L., Goldader, J.D., Leitherer, C., Schaerer, D., Oliva, E., 1999, apjj51496
- Origlia, L., Moorwood, A.F.M., Oliva, E., 1993, Astron. Astrophys., 280, 536.
- Ohsuga, K., Umemura, M., 1999, Ap. J. (Letters), 521, 13.
- Pérez-Olea, D.E., Colina, L., 1995, M.N.R.A.S., 277, 857.
- Regan, M.W., Mulchaey, J.S., 1999, A. J., 117, 2676.
- Rubin, V.C., Ford, W.K. 1968, Ap. J., 154, 431.
- Salamanca, I. et al., 1994, Astron. Astrophys., 282, 742.
- Salpeter, E. E., 1955, Ap. J., 121, 161.
- Sanders, D.B., Mirabel, I.F., 1996, Ann. Rev. Astron. Astrophys., 34, 749.
- Sanders, D.B., Phinney, E.S., Neugebauer, G., Soifer, B.T., Matthews, K., 1989, Ap. J., 347, 29.
- Scalo, J.M., 1986, Fundamentals of Cosmic Physics, vol. 11, 1
- Scalo, J.M., 1999, 'The Birth of Galaxies', Blois, France, in press, astro-ph/9811341
- Schinnerer, E., Eckart, A., Quirrenbach, A., Böker, T., Tacconi-Garman, L. E., Krabbe, A., Sternberg, A., 1997, Ap. J., 488, 174.
- Schinnerer, E., Eckart, A., Tacconi, L.J., 1999, Ap. J. (Letters), 524, L5.

- Schinnerer, E., Eckart, A., Tacconi, L.J., 2000, *Ap. J.*, 533, 826.
- Schmitt, H.R., Kinney, A.L., 1996, *Ap. J.*, 463, 498.
- Schmitt, H.R., Kinney, A.L., Calzetti, D., Storchi Bergmann, T., 1997, *A. J.*, 114, 592.
- Schreiber, N.M., 1998, Ph.D. thesis, LMU München
- Shlosman, I., Frank, J., Begelman, M.C., 1989, *Nature*, 338, 45
- Simpson, C., Forbes, D.A., Baker, A.C., Ward, M.J., 1996, *M.N.R.A.S.*, 283, 777.
- Stasińska, G., Leitherer, C., 1996, *Ap. J. Supp.*, 107, 734.
- Talon, S., Zahn, J.-P., Maeder, A., Meynet, G., 1997, *Astron. Astrophys.*, 322, 209.
- Tecza, M., Genzel, R., Tacconi, L.J., Anders, S., Tacconi-Garman, L.E., Thatte, N., 2000, *Ap. J.*, submitted, .
- Terlevich, E., Díaz, A.I., Terlevich, R., 1990, *M.N.R.A.S.*, 242, 271.
- Thatte, N.A., Kroker, H., Weitzel, L., Tacconi-Garman, L.E., Tecza, M., Krabbe, A., Genzel, R., 1995, *Proc. SPIE Vol. 2475*, 228
- Thatte, N., Quirrenbach, A., Genzel, R., Maiolino, R., Tecza, M., 1997, *Ap. J.*, 490, 238.
- Tielens, A.G.G.M., Hollenbach, D.J., 1985, *Ap. J.*, 291, 747.
- Van Bever, J., Vanbeveren, D., 1998, *Astron. Astrophys.*, 334, 21.
- Vanbeveren, D., De Donder, E., Van Bever, J., Van Rensbergen, W., De Loore, 1998, *New Astr.*, 3, 443
- Vanzi, L., Alonso-Herrero, A., Rieke, G.H., 1998, *Ap. J.*, 504, 93.
- Wallace, L., Hinkle, K., 1997, *Ap. J. Supp.*, 111, 445.
- Ward, M.J., Elvis, M., Fabbiano, G., et al., 1987, *Ap. J.*, 315, 74.
- Weitzel, L., Krabbe, A., Kroker, H., Thatte, N., Tacconi-Garman, L. E., Cameron, M., Genzel, R., 1996, *Astron. Astrophys. Suppl.*, 119, 531.
- Wilson, A.S., 1997, in "Emission Lines in Active Galaxies: New Methods and Techniques", *ASP Conf. Series*, Vol. 113, 264
- Winge, C., Peterson, B.M., Horne, K., Pogge, R.W., Pastoriza, M.G., Storchi-Bergmann, T., 1995, *Ap. J.*, 445, 680.

Table 1: Log of the NIR observations of NGC 3227

Camera		<i>J</i>	<i>H</i>	<i>K</i>	Observing run
3D	$T_{int}$		1840 s	3200 s	3.5 m CA, Dec. 1995
	$T_{int}$		1160 s	3910 s	WHT, Dec./Jan. 1995/96
	Seeing <sup>2</sup>		$\sim 1.6''$	$\sim 1.3''$	both runs
SHARP 1	$T_{int}$	3750 s	1900 s	4200 s	NTT, June 1996
	Seeing <sup>1</sup>	0.55''	0.35''	0.35''	NTT, June 1996

<sup>1</sup> derived from the PSF (reference star)

<sup>2</sup> derived from comparison of reference star and source data to SHARP 1 data

The integration times are on-source observing time. (NTT = New Technology Telescope, La Silla, Chile; 3.5 m CA = 3.5 m Telescope Calar Alto, Spain; WHT = William Herschel Telescope, La Palma, Spain)

Table 2: Data from the literature for the 3D data of NGC 3227

Line	Aperture	Flux <sub>3D</sub> <sup>c</sup> [10 <sup>-17</sup> W m <sup>-2</sup> ]	Flux <sub>lit</sub> [10 <sup>-17</sup> W m <sup>-2</sup> ]	Reference
H <sub>2</sub> 1-0 S(1)	5.4''	3.02 ± 0.17	3.3 ± 0.6	Fischer et al. 1987
H <sub>2</sub> 1-0 S(0)	5.4''	0.52 ± 0.11	2.1 ± 0.5	Fischer et al. 1987
H <sub>2</sub> 2-1 S(1)	5.4''	0.49 ± 0.15	2.6 ± 1.3	Fischer et al. 1987
Brγ <sup>a</sup>	5.4''	1.67 ± 0.41	~ 6.2	Fischer et al. 1987
[Fe II] <sup>b</sup>		4.91 ± 0.32	~ 10	Forbes & Ward 1993

Line	Aperture	EW <sub>3D</sub> <sup>c</sup> [Å]	EW <sub>lit</sub> [Å]	Reference
H <sub>2</sub> 1-0 S(1)	3.4'' × 12.0''	5.82 ± 0.33	6.0 ± 0.5	Vanzi et al. 1998
H <sub>2</sub> 1-0 S(0)	3.4'' × 12.0''	1.06 ± 0.22	3.0 ± 1.0	Vanzi et al. 1998
Brγ	3.4'' × 12.0''	3.30 ± 0.81	2.5 ± 0.5	Vanzi et al. 1998
He I	3.4'' × 12.0''	≤ 1.0	1.1 ± 0.5	Vanzi et al. 1998
[Fe II]	3.4'' × 12.0''	5.78 ± 0.38	3.5 ± 1.0	Vanzi et al. 1998

<sup>a</sup> Derived from the Paβ flux of Ward et al. (1987) and assuming Paβ/Brγ ≈ 6.

<sup>b</sup> Assuming [Fe II] 1.64 μm = 0.71 [Fe II] 1.24 μm using the value of Ward et al. 1987.

<sup>c</sup> Measured in a 4.6'' aperture.

Table 3: Fluxes and equivalent widths of the BLR, CLR and NLR emission lines in NGC 3227

Line	λ <sub>o</sub> [μm]	Flux [10 <sup>-17</sup> W m <sup>-2</sup> ]	EW [Å]
[FeII]	1.53	1.53 ± 0.34	2.02 ± 0.45
[FeII]	1.64	4.80 ± 0.15	6.33 ± 0.21
[FeII]	1.74	2.03 ± 0.24	2.92 ± 0.35
[SiVI] <sup>a</sup>	1.96	2.15 ± 0.17	2.46 ± 0.20
[AlIX]	2.04	0.75 ± 0.14	1.62 ± 0.30
Brγ	2.17	1.66 ± 0.26	3.66 ± 0.57

<sup>a</sup> possible contribution of the H<sub>2</sub>1-0 S(3) are not taken into account

Fluxes and equivalent widths (EW) of the emission lines of the BLR, CLR and NLR measured in a 3.6'' center on the nucleus of NGC 3227. The quoted uncertainties for the line fluxes include the uncertainties from the choice of the baseline for the continuum. The total absolute uncertainty is larger, since the calibration uncertainties will be added. The uncertainties for the equivalent widths were obtained from the uncertainties of the line fluxes and the corresponding neighboring continuum. The spatial resolution is 1.6'' (*H* band) and 1.3'' (*K* band). (10<sup>-14</sup> erg s<sup>-1</sup> cm<sup>-2</sup> = 10<sup>-17</sup> W m<sup>-2</sup>)

Table 4: Fluxes and equivalent widths of the stellar absorption lines in NGC 3227

Linie	$\lambda_o$ [ $\mu\text{m}$ ]	Flux [ $10^{-17} \text{ W m}^{-2}$ ]	EW [ $\text{\AA}$ ]
SiI	1.59	$-0.91 \pm 0.12$	$1.23 \pm 0.16$
CO 6-3	1.62	$-1.42 \pm 0.10$	$1.88 \pm 0.13$
CO 7-4	1.64	$-0.86 \pm 0.09$	$1.13 \pm 0.12$
CO 8-5	1.66	$-0.90 \pm 0.07$	$1.20 \pm 0.09$
CO 9-6	1.68	$-0.76 \pm 0.14$	$1.02 \pm 0.19$
CO 10-7	1.71	$-0.94 \pm 0.14$	$1.28 \pm 0.19$
Mg/Al	2.11	$-0.53 \pm 0.19$	$1.15 \pm 0.41$
NaI	2.21	$-1.47 \pm 0.19$	$3.27 \pm 0.42$
CaI	2.26	$-0.58 \pm 0.17$	$1.35 \pm 0.40$
$^{12}\text{CO}$ (2-0)	2.29	$-3.41 \pm 0.37$	$7.91 \pm 0.86$
$^{12}\text{CO}$ (3-1)	2.32	$-2.56 \pm 0.21$	$5.93 \pm 0.49$
$^{12}\text{CO}$ (4-2)	2.35	$-2.80 \pm 0.26$	$6.48 \pm 0.60$
$^{12}\text{CO}$ (5-3)	2.38	$-3.78 \pm 0.40$	$8.75 \pm 1.25$
$\sum ^{12}\text{CO}$		$-12.32 \pm 1.19$	$28.53 \pm 12.13$
CO		$-22.24 \pm 3.19$	$51.53 \pm 58.71$
$\frac{CO6-3}{SiI}$			$1.53 \pm 0.23$
$\frac{CO6-3}{CO2-0}$			$0.48 \pm 0.06$
$\log(\frac{CO6-3}{SiI})$			$0.18 \pm 0.07$
$\log(\frac{CO6-3}{CO2-0})$			$-0.32 \pm 0.06$

Fluxes and equivalent widths (EW) of the stellar absorption lines measured in a 3.6'' center on the nucleus of NGC 3227. The quoted uncertainties for the line fluxes include the uncertainties from the choice of the baseline for the continuum. The total absolute uncertainty is larger, since the calibration uncertainties will be added. The uncertainties for the equivalent widths were obtained from the uncertainties of the line fluxes and the corresponding neighboring continuum. The spatial resolution is 1.6'' ( $H$  band) and 1.3'' ( $K$  band). ( $10^{-14} \text{ erg s}^{-1} \text{ cm}^{-2} = 10^{-17} \text{ W m}^{-2}$ )

Table 5: NIR flux densities and colors of NGC 3227 at a resolution of 0.55''

Aper. [']	J		H		K		J - H [mag]	H - K [mag]	J - K [mag]
	[mJy]	[mag]	[mJy]	[mag]	[mJy]	[mag]			
0.6	6.57	13.58	9.84	12.59	13.06	11.71	0.98	0.88	1.87
1.0	14.63	12.71	21.19	11.76	26.61	10.94	0.95	0.82	1.77
1.4	22.43	12.24	31.07	11.34	37.18	10.57	0.90	0.77	1.67
1.8	29.45	11.95	39.31	11.09	45.39	10.36	0.86	0.73	1.59
2.2	35.68	11.74	46.40	10.91	52.23	10.21	0.83	0.70	1.53
2.6	41.06	11.59	52.49	10.77	58.02	10.09	0.81	0.68	1.50
3.0	45.74	11.47	57.84	10.67	63.09	10.00	0.80	0.67	1.47
3.6	51.91	11.33	64.84	10.55	69.65	9.89	0.79	0.65	1.44
4.6	60.53	11.17	74.58	10.39	78.67	9.76	0.77	0.63	1.40
6.0	70.51	11.00	85.71	10.24	89.07	9.63	0.76	0.62	1.37
9.0	87.79	10.76	105.05	10.02	107.94	9.42	0.74	0.60	1.34
9.1	88.27	10.76	105.62	10.02	108.51	9.41	0.74	0.60	1.34

NIR flux densities and colors measured in different apertures center on the nucleus of NGC 3227. The calibration uncertainties in each band for the individual nights are 7.8 % (*J* band), 4.8 % (*H* band) and 5.7 % (*K* band). Additional uncertainties from the calibration of the standard star 35 Leo as well as systematic uncertainties amount in a total uncertainty for each band of about 10%.

Table 6: Flux values of the northern knot

Band	[mJy]	[mag]
V	0.07	19.37
J	0.33	16.82
H	0.42	16.02
K	0.39	15.52

Values are measured in a 1'' aperture centered in the middle of the extended structure. The uncertainties correspond to the ones mentioned in Table 5. The uncertainties of the HST *V* band are higher, since only a differential calibration has been possible (see text).

Table 7: Star Formation Scenarios in the Nucleus

	Obs.	RSG <sup>a</sup>	RSG <sup>b</sup>	RSG <sup>c</sup>	AGB <sup>d</sup>	RG <sup>e</sup>
% M stars (H)	30	38	33	40	27	27
% M stars (K)	25	24	22	11	12	12
% stellar (H)	65	65	65	65	65	65
% stellar (K)	40	40	40	40	40	40
$L_K$ [ $10^8 L_\odot$ ]	1.4	1.4	1.4	1.4	1.4	1.4
$L_{LyC}$ [ $10^8 L_\odot$ ]	3.9 <sup>1</sup>	2.3	0.3	0.0	0.0	3.3
$L_{bol}$ [ $10^9 L_\odot$ ]	9.3	10.0	12.5	9.0	3.6	6.2
$\nu_{SN}$ [ $10^{-2} \text{ yr}^{-1}$ ]	2.4	2.3	5.0	0.2	0.0	0.4
$m_{st}$ [ $10^8 M_\odot$ ]	11 <sup>2</sup>	0.3	0.9	1.5	3.7	5.6
$m_{gas}$ [ $10^8 M_\odot$ ]	0.9	0.4	1.2	2.4	8.2	26
SFR [ $10^{-2} \text{ yr}^{-1}$ ]		9.1	0.9	0.0	0.0	26.8

<sup>1</sup> total observed Br $\gamma$  flux used

<sup>2</sup> dynamical mass in the inner 3.6'' derived from the rotation curve (Schinnerer, Eckart & Tacconi 2000)

The observed values are derived assuming  $A_V=4^{mag}$  and using the following measured values in a 3.6'' aperture:  $S_K=27.9\text{mJy}$ ,  $S_{5GHz}=24\text{mJy}$ ,  $F_{Br\gamma}=1.66\times 10^{-14} \text{ ergs cm}^{-2}$ . The equations can be found in section A.3.  $m_{st}$  and  $m_{gas}$  denote the present-day stellar mass and the consumed gas mass to date, respectively.

All starburst models are calculated using a Salpeter IMF with mass cut-offs of  $0.8 M_\odot$  to  $120 M_\odot$ .

RSG<sup>a</sup>: age of 15 Myr and decay time of 3 Myr

RSG<sup>b</sup>: age of 25 Myr and decay time of 3 Myr

RSG<sup>c</sup>: age of 50 Myr and decay time of 3 Myr

AGB<sup>d</sup>: age of 0.5 Gyr and decay time of 3 Myr

RG<sup>e</sup>: age of 10 Gyr and continuous star formation.



Table 8: Variation of the model parameters

Fig.	Variied parameter	$m_{up}$ [ $M_{\odot}$ ]	kind	$t_{burst}$ [ $10^7$ yr]	$A_V$ [mag]	dust in % of $K$ band flux
15 (a), (e)	age	120	decaying	0.7	0.0	0.0
	age	120	decaying	1.56	0.0	0.0
	age	120	decaying	7.0	0.0	0.0
	age	120	constant	700.0	0.0	0.0
15 (b), (f)	$m_{up}$	120	decaying	0.7	0.0	0.0
	$m_{up}$	30	decaying	0.7	0.0	0.0
	$m_{up}$	10	decaying	0.7	0.0	0.0
15 (c), (g)	$A_V$	120	decaying	1.56	0.0	0.0
	$A_V$	120	decaying	1.45	5.0	0.0
	$A_V$	120	decaying	1.56	10.0	0.0
15 (d), (h)	dust	120	decaying	1.56	0.0	0.0
	dust	120	decaying	1.56	0.0	10.0
	dust	120	decaying	1.56	0.0	25.0

Variied parameters in Figure 15 for  $H$  and  $K$  band spectra. Age ( $t_{burst}$ ), upper mass cut-off ( $m_{up}$ ), kind of burst as well as extinction ( $A_V$ ) and contribution of hot dust emission (with a temperature of 900 K) to the  $K$  band flux were changed.

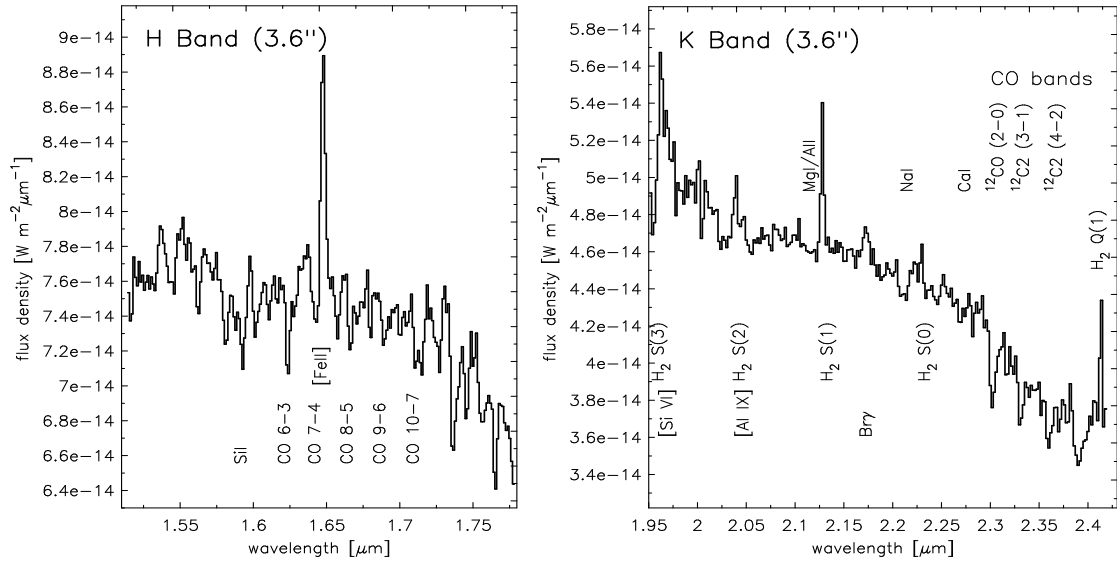


Fig. 1.— 3D spectra of NGC 3227 in *H* and *K* band in a circular aperture of 3.6".

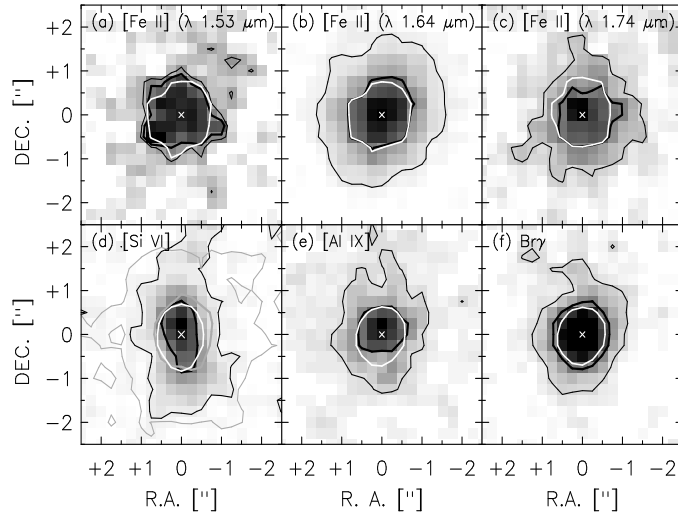


Fig. 2.— Maps of the AGN emission lines in the nucleus of NGC 3227. The 50% contour lines of the line emission (fat black line) and the neighboring continuum (fat white line) are shown. The thin black line indicates the  $3\sigma$  level in the maps. In the [Si VI] line image (d) the corresponding contours of the neighboring H<sub>2</sub>1-0 S(3) line are shown as well to demonstrate the different spatial extend of both lines (50% contour line: fat gray line;  $3\sigma$  level: thin gray line). For further discussion see text.

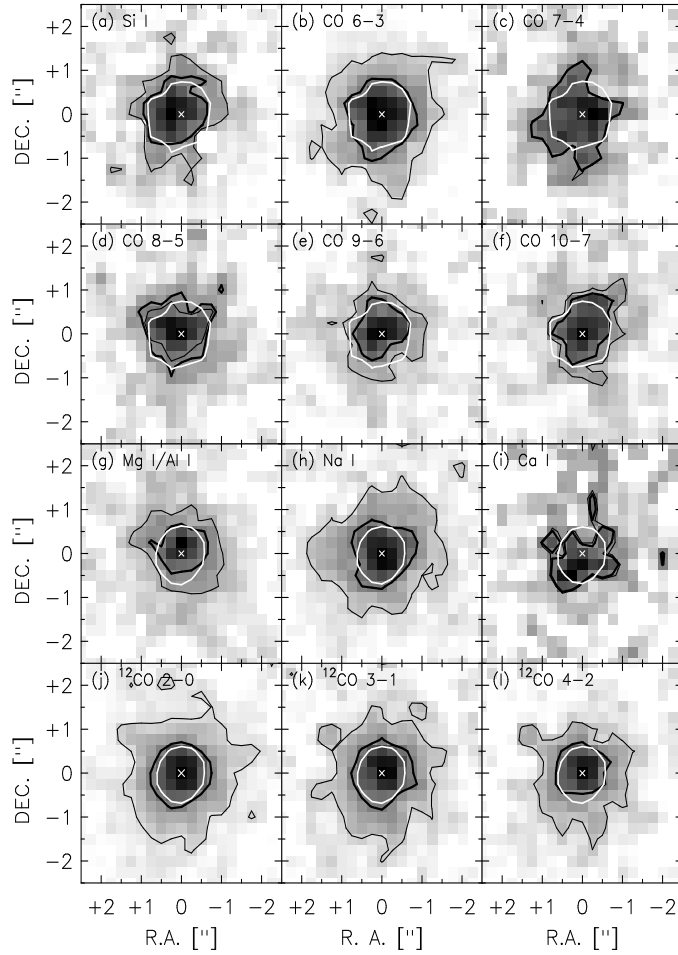


Fig. 3.— Maps of the extended stellar absorption lines in the nucleus of NGC 3227. The 50% contour lines of the line absorption (fat black line) and the neighboring continuum (fat gray line) are shown. The thin black line indicates the  $3\sigma$  level in the maps.

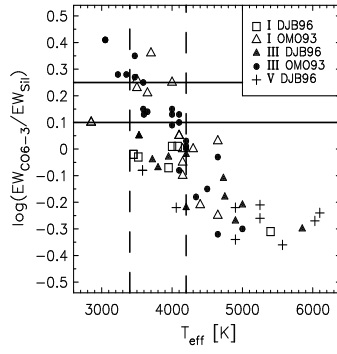


Fig. 4.— Diagnostic line diagram for NGC 3227. The observed range of the  $\log(\frac{\text{CO6-3}}{\text{SiI}})$  is indicated (fat solid lines). The resulting range for the effective temperature is given by the broken lines. (DJB96: Dallier, Boisson, July 1996; OMO93: Origlia, Moorwood, Oliva 1993)

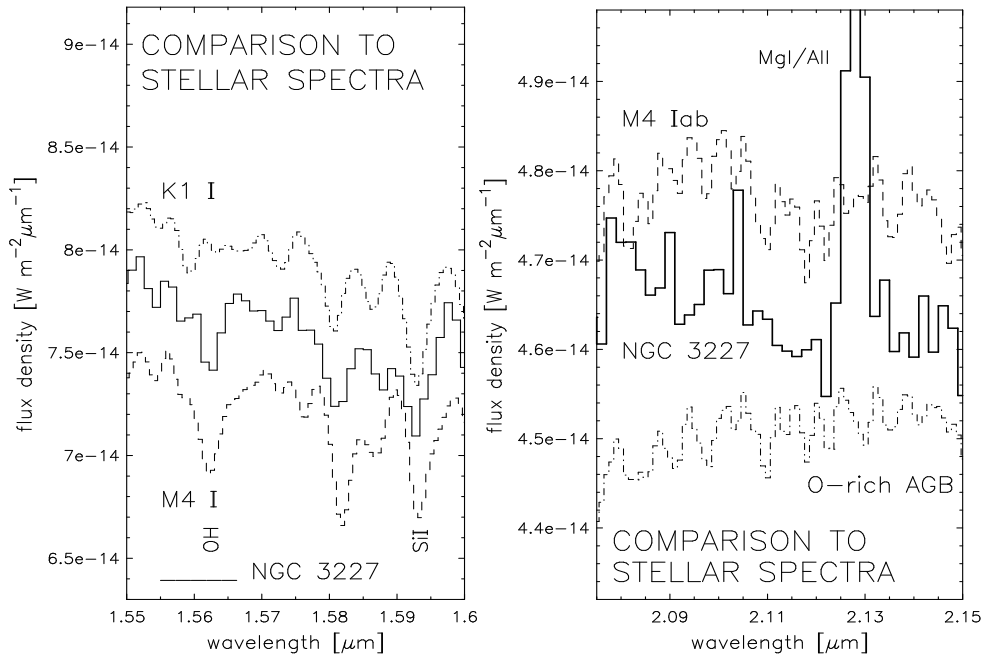


Fig. 5.— Comparison of the OH line in NGC 3227 to standard star spectra (K1 I: 93 Her, M4 I: HR 921; from Meyer et al. 1998). Comparison of the *K* band spectrum of NGC 3227 to spectra of an AGB star and a supergiant (S6+/le:  $\chi$  Cyg, M3-4 Iab: SU Per; from Wallace & Hinkle 1997) scaled and continuum added according the line depths.

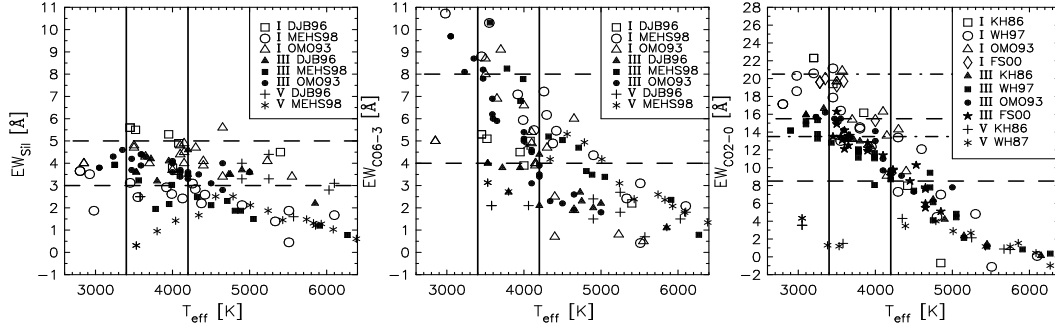


Fig. 6.— Determination of the luminosity class in NGC 3227. The equivalent widths of Si I (left), CO 6-3 (middle) and CO 2-0 (right) for different effective temperatures are shown. In each diagram the obtained temperature range from the  $\frac{CO6-3}{SiI}$  ratio is indicated (fat solid lines). The expected line ratios are shown by broken lines (right figure: giants (broken line), supergiants (dashed-dotted line)). (DJB96: Dallier, Boisson, Joly 1996; MEHS98: Meyer et al. 1998; OMO93: Origlia, Moorwood, Oliva 1993; KH86: Kleinmann & Hall 1986; WH97: Wallace & Hinkle 1997; FS00: Förster Schreiber 2000))

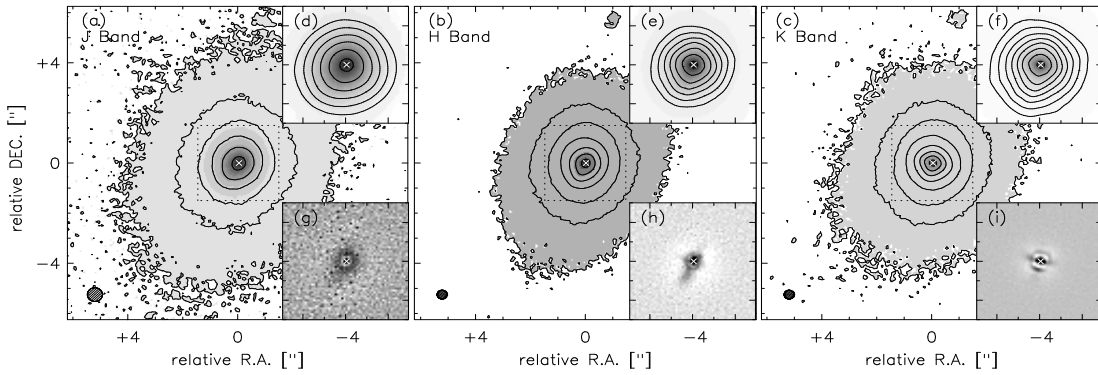


Fig. 7.— *J*, *H* and *K* band SHARP maps and smooth-subtracted maps of NGC 3227. For comparison the contours of the PSF reference star are overlaid on the maps of NGC 3227 (d - f). In the smooth-subtracted maps (g - i) no prominent structure is seen. (a) *J* band at  $0.55''$  resolution: contour lines are at 2, 4, 8, 16, 32, 64 and 100% of the maximum intensity of  $0.08$  mJy/pixel (1 Pixel =  $0.05'' \times 0.05''$ ) (b) *H* band at  $0.35''$  resolution: contour lines are at 1, 2, 4, 8, 16, 32, 64 and 100% of the maximum intensity of  $0.19$  mJy/pixel (1 Pixel =  $0.05'' \times 0.05''$ ) (c) *K* band at  $0.35''$  resolution: contour lines are at 0.5, 1, 2, 4, 8, 16, 32, 64 and 100% of the maximum intensity of  $0.35$  mJy/pixel (1 Pixel =  $0.05'' \times 0.05''$ ). The contours for the reference star are identical to the contours for NGC 3227 in the maps with a larger FOV. The smooth-subtracted maps of the *J* (g), *H* (h) and *K* (i) band show a  $3''$  FOV.



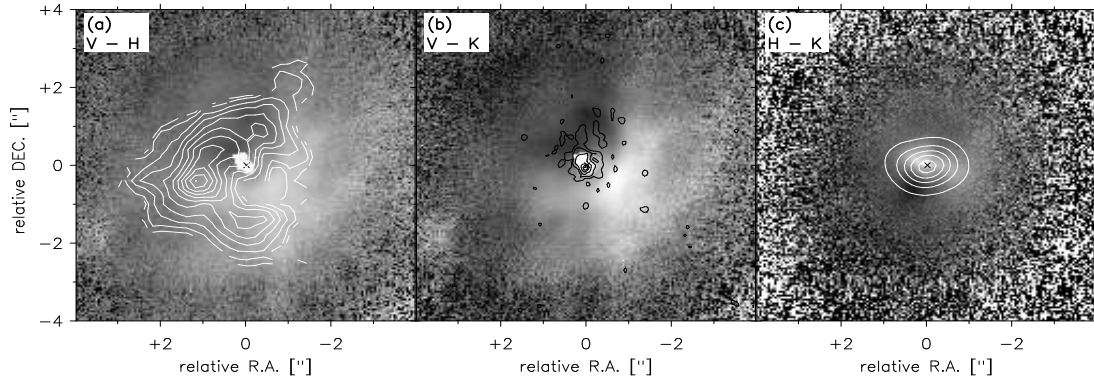


Fig. 8.—  $V - H$ ,  $V - K$  and  $H - K$  color maps of NGC 3227 using the HST and SHARP1 data at an angular resolution of  $0.35''$ . White in the figure corresponds to redder colors in the galaxy. The  $[\text{O III}]$  line emission from Schmitt & Kinney (1996) is shown in the  $V - K$  map in contours of 0.5, 2, 8, 32, 64 and 100% of the maximum. The molecular line emission of  $^{12}\text{CO}$  2-1 is shown in the  $V_H$  map in contours of 5, 10, 20, ... 100% of the maximum (from Schinnerer, Eckart & Tacconi 2000). The deconvolved  $\text{H}_2$  1-0 S(1) line map at a resolution of  $0.8''$  is shown in contours of 10, 30, ... 90 % of the maximum in the  $H - K$  map. In the  $V - H$  and  $V - K$  maps a red ring is visible in bright gray tone around the nucleus. In direction of the ionization cone ( $[\text{O III}]$  contours towards north-east) this ring is bluer. The red east-west extension of the nucleus in the  $H - K$  map is in agreement with the extended  $\text{H}_2$  line emission and stellar absorption lines. The  $0.5''$  diameter ring is likely the first diffraction ring.

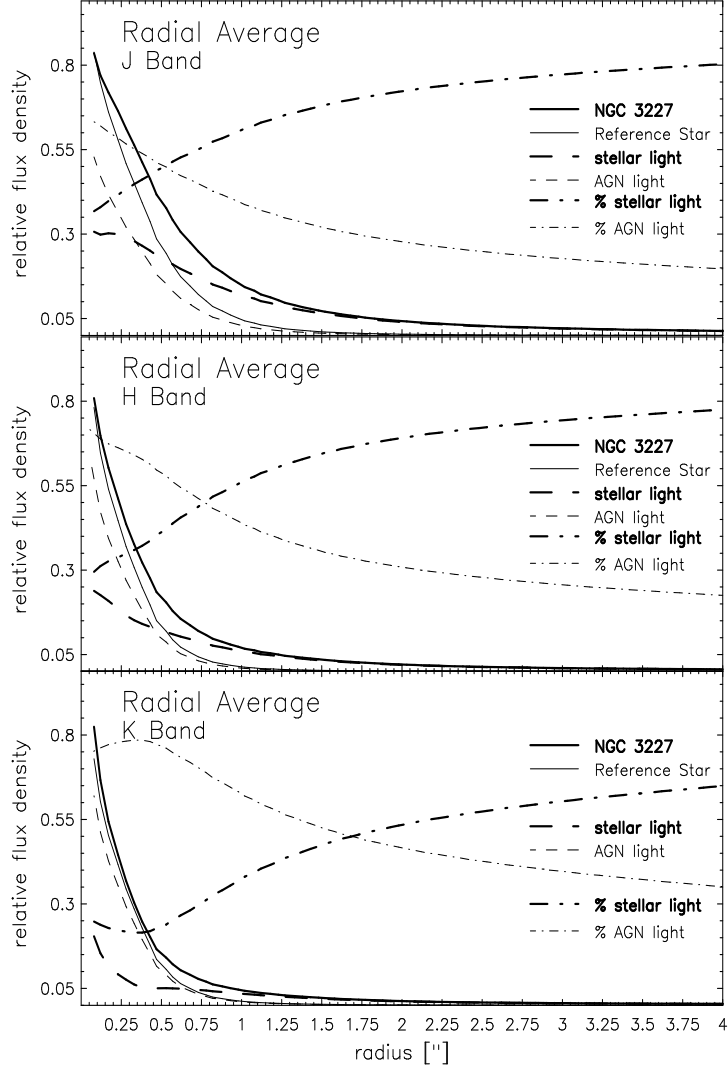


Fig. 9.— Comparison of the radial averages of the flux density distribution in NGC 3227 (fat solid line) to the reference star (PSF) (thin solid line) in the NIR *JHK* bands. To estimate the contribution of the nuclear stellar cluster mapped in its absorption lines (see section 4), we subtracted the PSF representing the AGN emission from the observed profile. The resulting stellar light profile (fat broken line) and AGN profile (thin broken line) are shown as well. The FWHM of the stellar light profile is  $\sim 0.9''$  if we account for the underlying bulge light. This size is similar to the FWHM measured in the absorption line maps (see Fig. 3). In addition the relative contribution of the stellar light (fat dashed-dotted line) and the AGN emission (thin dashed-dotted line) to the total flux density within each radius is shown. The radial averages were calculated in steps of one pixel ( $0.05''$ ) to obtain a good sampling of the PSF and the galaxy nucleus. For comparison the curves were normalized to one.

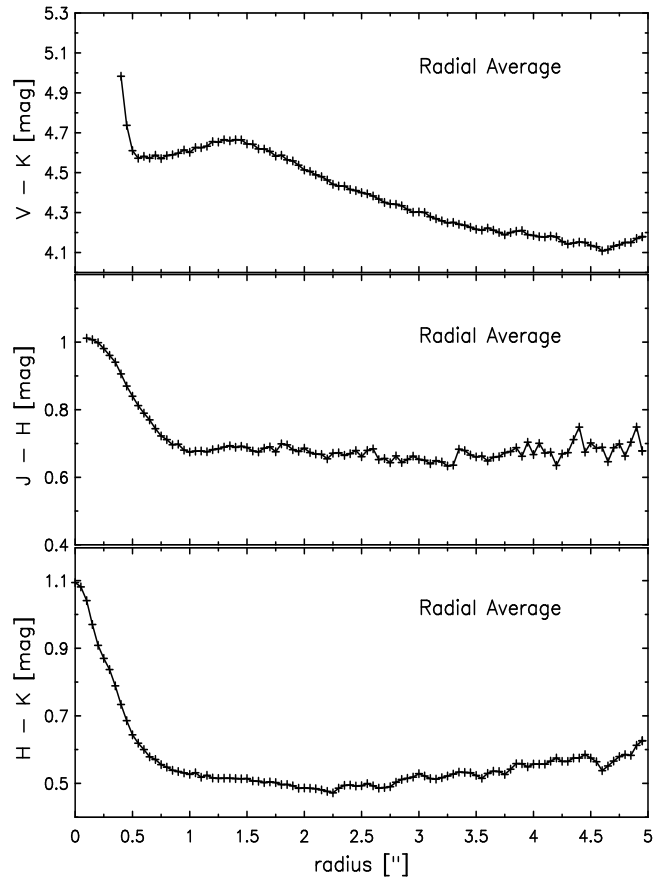


Fig. 10.— Comparison of the radial averages of the colors in NGC 3227. The radial averages of the flux densities were used to obtain the colors. Due to the saturated nucleus in the HST image, the  $V - K$  color can only be derived for radii  $\geq 0.35''$ .

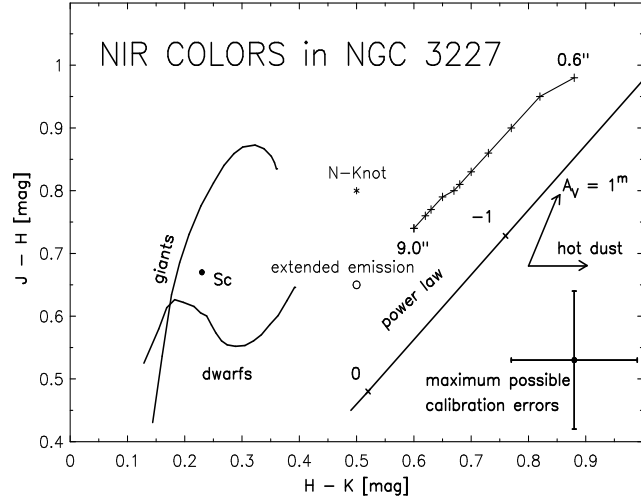


Fig. 11.— NIR  $JHK$  diagram of NGC 3227 in full apertures of different size (apertures of 0.6", 1.0", 1.4", 1.8", 2.2", 2.6", 3.0", 3.6", 4.6", 6.0", 9.0" measured in the SHARP maps). Values of the northern knot (star) and the extended emission (o) at a radius of 1.0" are shown in addition. For comparison the typical colors of late dwarf and giant stars as well as the typical colors of a Sc galaxy (Frogel et al. 1978) are indicated. The expected contributions of extinction and hot dust emission as well as the power law for pure AGN emission are shown.

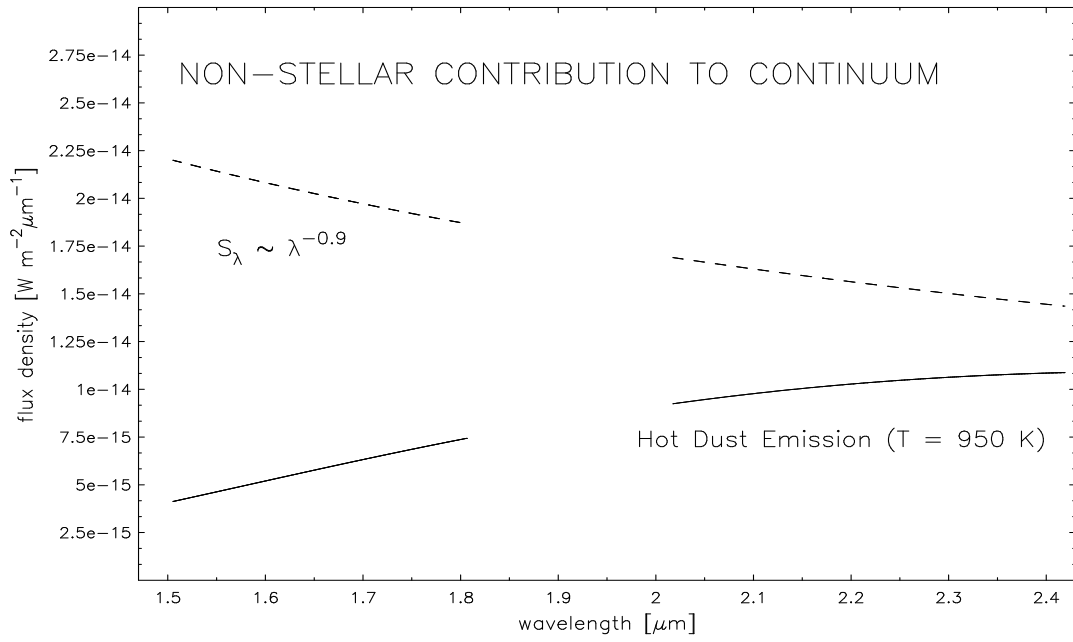


Fig. 12.— The non-stellar contributions to the continuum in the  $H$  and  $K$  band for NGC 3227. The contribution of a 900 K hot dust emission (solid line) and of the non-thermal AGN contribution (broken line) are shown.

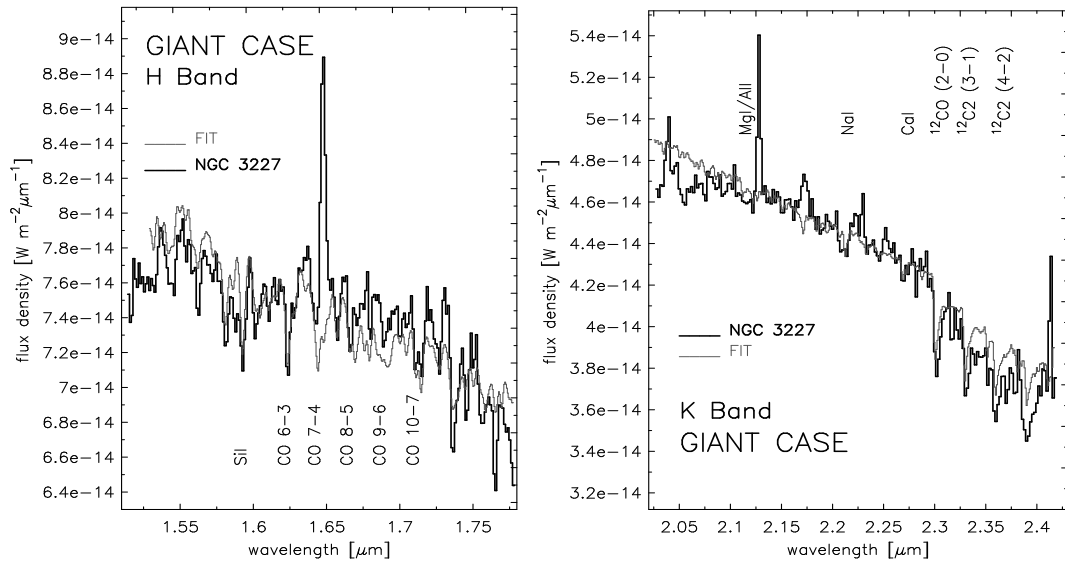


Fig. 13.— SPECSYN result of the RG (red giants) scenario for NGC 3227. The agreement between the data (black line) and the synthetic spectrum (gray line) is satisfying.

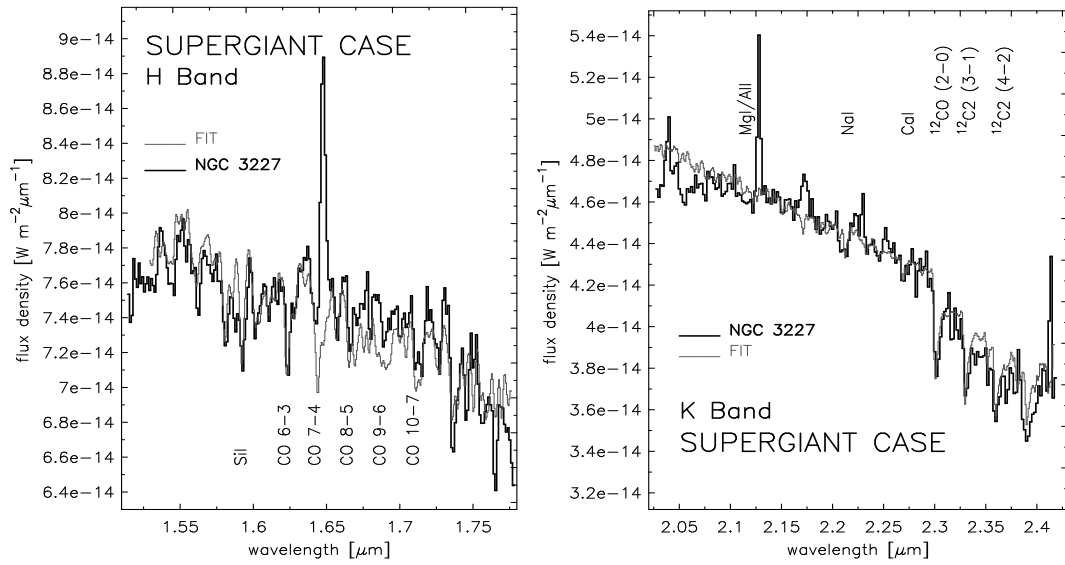


Fig. 14.— SPECSYN result of the RSG (red supergiants) scenario for NGC 3227. The agreement between the data (black line) and the synthetic spectrum (gray line) is good.

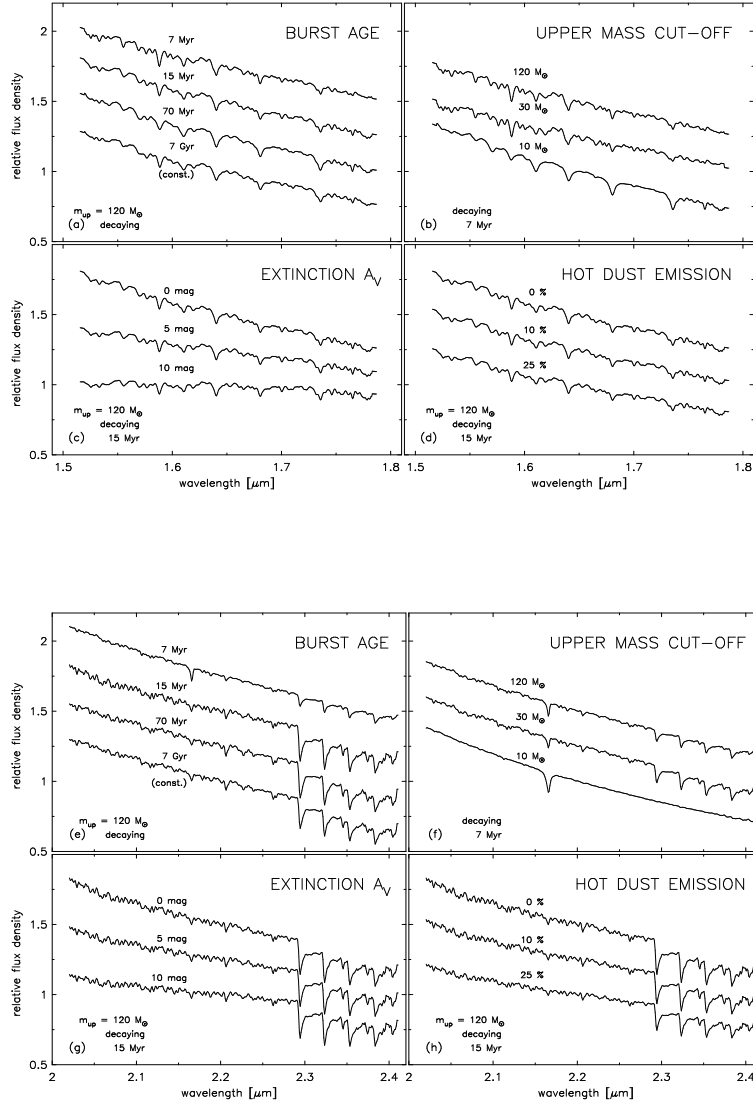


Fig. 15.— Influence of the different model parameter for the  $H$  band (a - d) and  $K$  band (e - h) synthesized spectra of stellar clusters. All spectra are normalized to one at  $1.65 \mu\text{m}$  and  $2.2 \mu\text{m}$ , respectively, and moved by  $0.25$  for display. An overview of the varied model parameter is presented in Table 8.